

The effects of age on resting-state BOLD signal variability is explained by cardiovascular and cerebrovascular factors

KAMEN A. TSVETANOV^{1,2,*}, RICHARD N.A. HENSON^{3,4}, P. SIMON JONES², HENK-JAN MUTSAERTS⁵, DELIA FUHRMANN³, LORRAINE K. TYLER², CAM-CAN^{1,2} AND JAMES B. ROWE^{2,3}

* Corresponding author (kat35@cam.ac.uk, +44 1223 766 556)

¹ Department of Clinical Neurosciences, University of Cambridge, Cambridge, UK

² Centre for Speech, Language and the Brain, Department of Psychology, University of Cambridge, Cambridge, UK

³ Medical Research Council Cognition and Brain Sciences Unit, Cambridge, UK

⁴ Department of Psychiatry, University of Cambridge, Cambridge, UK

⁵ Department of Radiology and nuclear medicine, Amsterdam University Medical Center, Amsterdam, The Netherlands

Summary: Accurate identification of brain function is necessary to understand neurocognitive ageing, and thereby promote health and well-being. Many studies of neurocognitive aging have investigated brain function with the blood-oxygen level-dependent (BOLD) signal measured by functional magnetic resonance imaging. However, the BOLD signal is a composite of neural and vascular signals, which are differentially affected by aging. It is therefore essential to distinguish the age effects on vascular *versus* neural function. The BOLD signal variability at rest (known as resting state fluctuation amplitude, RSFA), is a safe, scalable and robust means to calibrate vascular responsivity, as an alternative to breath-holding and hypercapnia. However, the use of RSFA for normalization of BOLD imaging assumes that age differences in RSFA reflecting only vascular factors, rather than age-related differences in neural function (activity) or neuronal loss (atrophy). Previous studies indicate that two vascular factors, cardiovascular health and cerebrovascular function, are insufficient when used alone to fully explain age-related differences in RSFA. It remains possible that their joint consideration is required to fully capture age differences in RSFA. We tested the hypothesis that RSFA no longer varies with age after adjusting for a combination of cardiovascular and cerebrovascular measures. We also tested the hypothesis that RSFA variation with age is not associated with atrophy. We used data from the population-based, lifespan Cam-CAN cohort. After controlling for cardiovascular and cerebrovascular estimates alone, the residual variance in RSFA across individuals was significantly associated with age. However, when controlling for both cardiovascular and cerebrovascular estimates, the variance in RSFA was no longer associated with age. Grey matter volumes did not explain age-differences in RSFA, after controlling for cardiovascular health. The results were consistent between voxel-level analysis and independent component analysis. Our findings indicate that cardiovascular and cerebrovascular signals are together sufficient predictors of age differences in RSFA. We suggest that RSFA can be used to separate vascular from neuronal factors, to characterise neurocognitive aging. We discuss the implications and make recommendations for the use of RSFA in the research of aging.

Keywords (up to five): *ageing, functional magnetic resonance imaging (fMRI), individual differences, cerebral vascular reactivity*

1. Introduction

The worldwide population is rapidly aging with an increasing number and proportion of older adults across the globe (Beard et al., 2016). Considering the cognitive decline and increasing burden of dementia in aging societies, there is a pressing need to understand the neurobiology of cognitive aging. This will inform efforts to maintain mental wellbeing into late life, allowing people to work and live independently for longer. Research in cognitive neuroscience of aging has used blood-oxygen level-dependent (BOLD) signal measured by functional magnetic resonance imaging (fMRI) as one of the standard ways to examine the neural mechanisms of cognition. However, the BOLD signal measures the activity of neurons indirectly through changes in regional blood flow, volume and oxygenation. This makes BOLD a complex convolution of neural and vascular signals, which are differentially affected by aging (Logothetis, 2008). Without careful correction for age differences in vascular health, differences in fMRI signals can be erroneously attributed to neuronal differences (Liu et al., 2013; Tsvetanov et al., 2015) and their behavioural relevance overstated (Geerligs et al., 2017; Geerligs and Tsvetanov, 2016; Tsvetanov et al., 2016).

It is possible to control for vascular differences in fMRI signal using additional baseline measures of cerebrovascular reactivity, including CO₂-inhalation-induced hypercapnia (Liu et al., 2019), breath-hold-induced hypercapnia (Handwerker et al., 2007; Mayhew et al., 2010; Riecker et al., 2003; Thomason et al., 2007, 2005), hyperventilation-induced hypocapnia (Bright et al., 2009; Krainik et al., 2005), and cerebral blood flow (CBF) or venous oxygenation measures (Liau and Liu, 2009; Lu et al., 2010; Restom et al., 2007). However, such methods have not been widely used, in part to impracticalities in large-scale studies, and poor tolerance by older adults (for a review see Tsvetanov et al., 2020). Additionally, a hypercapnic challenge may not be neuronally neutral, given participants' awareness of the aversive challenge, which may differ with age (Hall et al., 2011). Breath-hold compliance may also decrease with age (Jahani et al., 2017). Such biases affect data quality and

reliability measures (Magon et al., 2009), highlighting the advantage of non-invasive and “task-free” estimates of vascular components in the BOLD time series.

The BOLD signal variability in a resting state (“task-free”) is one such estimate and is also known as resting state fluctuation amplitudes (RSFA) (for a review see Tsvetanov et al., 2020). It has been proposed as a safe, scalable and robust cerebrovascular reactivity mapping technique (Golestani et al., 2016; Jahanian et al., 2014; Kannurpatti and Biswal, 2008; P. Liu et al., 2017). The use of RSFA as a normalization method for BOLD follows the assumption that age differences in RSFA reflect only vascular factors, rather than age-related differences in neural function or neuronal loss (atrophy). Fluctuations in the BOLD signal are associated with fluctuations in cardiac rhythm (Glover et al., 2007) that are independent of those associated with respiratory rate and depth (Chang et al., 2013, 2009), suggesting that RSFA may be susceptible to vascular signals of varying aetiologies, such as cardiovascular and cerebrovascular factors. Evidence in support of cardiovascular factors comes from Tsvetanov and colleagues (Tsvetanov et al., 2015, but also Makedonov et al., 2013; Viessmann et al., 2017, 2019; Theyers et al., 2018), who demonstrated that age-related differences in RSFA are mediated by cardiovascular health (as measured by pulseoximetry and electrocardiography, ECG), but not by neural function in terms of neural variability (as measured by magnetoencephalography, MEG). Evidence in support of cerebrovascular factors comes from Garrett et al. (2017) who found that “gold-standard” measures of cerebrovascular function (arterial spin labelling, ASL, and CO₂ inhalation-induced hypercapnia) are associated with RSFA. Importantly, both studies reported age-related differences in RSFA that remain after adjusting for individual differences in either cardiovascular or cerebrovascular factors. However, neither study considered jointly cardiovascular and cerebrovascular factors, and it remains unclear whether the unexplained age-related differences in RSFA reflect joint contributions from cardiovascular and cerebrovascular factors, as in the case of BOLD signal fluctuations (Chang et al., 2013, 2009). Alternatively, the unexplained age differences in RSFA may reflect neuronal factors, such as atrophy (Grady and Garrett, 2013), even though variation in neuronal activity does not explain the effect of age on RSFA (Tsvetanov et al., 2015).

Cardiovascular, cerebrovascular and other physiological signals, but not neuronal signals, contribute to the age-related differences in RSFA, yet none of these non-neuronal measures on their own could fully account for the effects of age on RSFA. It is possible that various vascular signals contribute to different components of the age effects on RSFA (Tsvetanov et al., 2020). However, no study to date has tested whether the cardiovascular and cerebrovascular signals together fully capture the effects of age on RSFA – an assumption underlying the use of RSFA as a scaling method. In this study we sought to investigate the effects of age on RSFA by the simultaneous assessment of the independent and shared effects of cardiovascular, cerebrovascular and neuronal effects on age-related differences in RSFA. To this end, we used a set of cardiovascular, cerebrovascular and volumetric measures in a population-based study of healthy ageing (age 18-88, N > 250, www.cam-can.org). We hypothesized that age-related variation in RSFA are predicted by cardiovascular and cerebrovascular factors, but not grey matter volume, and therefore that the residuals in RSFA – after adjusting for these vascular factors – are not associated with age.

2. Methods

2.1. Participants

Figure 1 illustrates the study design and image processing, using the Cambridge Centre Aging and Neuroscience dataset (Cam-CAN). Ethical approval was granted by Cambridgeshire 2 Research Ethics Committee. Participants gave written informed consent. A detailed description of exclusion criteria can be found in Shafto et al. (Shafto et al., 2014), including poor vision (below 20/50 on Snellen test; Snellen, 1862) or hearing (threshold 35dB at 1000Hz in both ears), ongoing or serious past drug abuse as assessed by the Drug Abuse Screening Test (DAST-20; Skinner, 1982), significant psychiatric disorder (e.g. schizophrenia, bipolar disorder, personality disorder) or neurological disease (e.g. stroke, epilepsy, traumatic brain injury). At an initial home assessment (Phase I), completed the Mini-Mental State Examination (MMSE > 25; Folstein et al., 1975) and Edinburgh Handedness Inventory (Oldfield, 1971). Participants attended MRI (T1-weighted, arterial spin labelling (ASL), FLAIR-based white matter

hyperintensities, resting state EPI-BOLD and field-map images) and MEG (including resting state ECG-recording) on two occasions (Phase II and III) separated by approximately 1 year. We include here 226 full datasets of good quality, required for all analysis (e.g. T1-weighted, FLAIR, ASL, resting fMRI and ECG recordings, see below). Demographic characteristics of the sample are described in Table 1. Imaging data were acquired using a 3T Siemens TIM Trio.

2.2. T1w image acquisition and processing

A 3D-structural MRI was acquired for each participant using T1-weighted Magnetization-Prepared Rapid Gradient-Echo (MPRAGE) sequence with Generalized Autocalibrating Partially Parallel Acquisition (GRAPPA) acceleration factor 2; Repetition Time (TR) = 2250ms; Echo Time (TE) = 2.99ms; Inversion Time (TI) = 900ms; flip angle $\alpha = 9^\circ$; field of view (FOV) = 256mm x 240mm x 192mm; resolution = 1mm isotropic) with acquisition time of 4 minutes and 32 seconds.

All image processing was done using Automatic Analysis (AA 4.0; Cusack et al., 2014; <https://github.com/automaticanalysis/automaticanalysis>) implemented in Matlab (Mathworks, <https://uk.mathworks.com/>). The results here come from Release004 of the CamCAN pipelines. Each participant's T1 image was coregistered to the MNI template in SPM12 (<http://www.fil.ion.ucl.ac.uk/spm>; Friston et al., 2007), and the T2 image was then coregistered to the T1 image using a rigid-body transformation. The coregistered T1 and T2 images underwent multi-channel segmentation (SPM12 Segment; Ashburner and Friston, 2005) to extract probabilistic maps of 6 tissue classes: GM, WM, cerebrospinal fluid (CSF), bone, soft tissue, and background. The native-space GM and WM segmentations were used for diffeomorphic registration (DARTEL; Ashburner, 2007) to create whole group template images (Taylor et al., 2015). The group template was normalised to the MNI space using 12-parameter affine transformation.

2.3. fMRI image acquisition and processing

RSFA was estimated from resting state Echo-Planar Imaging (EPI) of 261 volumes acquired with 32 slices (sequential descending order), slice thickness of 3.7 mm with a slice gap of 20% for whole

brain coverage (TR = 1970ms; TE = 30ms; flip angle $\alpha = 78^\circ$; FOV = 192mm x 192mm; resolution = 3mm x 3mm x 4.44mm) during 8 minutes and 40 seconds. Participants were instructed to lay still with their eyes closed. The initial six volumes were discarded to allow for T1 equilibration. We quantified participant motion using the root mean square volume-to-volume displacement as per Jenkinson et al (2002). The rs-fMRI data were further pre-processed by wavelet despiking (see below).

The EPI data were unwarped (using field-map images) to compensate for magnetic field inhomogeneities, realigned to correct for motion, and slice-time corrected to the middle slice. The normalisation parameters from the T1 image processing were then applied to warp functional images into MNI space. We applied data-driven wavelet-despiking to minimise motion artefacts (Patel et al., 2014). We observed a high association between the amount of outlying wavelet coefficient and head motion across subjects ($r = .739$, $p < .001$), demonstrating that it captured a large amount of motion artefacts in the data. Spatially normalised images were smoothed with a 12 mm FWHM Gaussian kernel. A general linear model (GLM) of the time-course of each voxel was used to further reduce the effects of noise confounds (Geerligs et al., 2017), with linear trends and expansions of realignment parameters, plus average signal in WM and CSF, their derivative and quadratic regressors (Satterthwaite et al., 2013). The WM and CSF signal was created by using the average across all voxels with corresponding tissue probability larger than 0.7 in associated tissue probability maps available in SPM12. A band-pass filter (0.0078-0.1 Hz) was implemented by including a discrete cosine transform set in the GLM, ensuring that nuisance regression and filtering were performed simultaneously (Hallquist et al., 2013; Lindquist et al., 2019). Finally, we calculated subject specific maps of RSFA based on the normalized standard deviation across time for processed resting state fMRI time series data.

2.4. ASL image acquisition and processing

To assess resting cerebral blood flow, we used pulsed arterial spin labelling (PASL, PICORE-Q2T-PASL in axial direction, 2500ms repetition time, 13ms echo time, bandwidth 2232 Hz/Px, 256 x 256 mm² field of view, imaging matrix 64x64, ten slices, 8 mm slice thickness, flip angle 90°, 700 ms inversion

time (TI) 1, TI2 = 1800 ms, 1600 ms saturation stop time). The imaging volume was positioned to maintain maximal brain coverage with a 20.9 mm gap between the imaging volume and a labelling slab with 100mm thickness. There were 90 repetitions giving 45 control-tag pairs (duration 3'52"). In addition, a single-shot EPI (M0) equilibrium magnetization scan was acquired. Pulsed arterial spin labelling time series were converted to cerebral blood flow (CBF) maps using ExploreASL toolbox (Mutsaerts et al., 2018). Following rigid-body alignment, the spatial normalised images were smoothed with a 12 mm FWHM Gaussian kernel.

2.5. Cardiovascular measures

2.5.1. Physiological recordings

Cardiac activity data were acquired using bipolar ECG while acquiring the MEG data, and processed using PhysioNet Cardiovascular Signal Toolbox (Goldberger et al., 2000; Vest et al., 2018) in Matlab (MATLAB 2017b, The MathWorks Inc, Natick, MA). To address non-stationarity in ECG recordings, mean heart rate (HR) and heart rate variability (HRV) summary measures were based on the median across multiple sliding 5-min windows in 30-second steps across the entire eyes-closed, resting-state acquisition, 8.5 minutes. Estimation of mean heart rate (HR) was based on the mean number of successive N-N (normal-to-normal) intervals within each 60-second interval during each 5-minute period recording. To estimate the HRV, we used the frequency-domain information of normal-to-normal (NN) intervals, which provides a measure of low- and high- frequency components of the HRV (unlike time-domain alternatives e.g. the root mean squared difference of successive intervals (RMSSD), which pertain mainly to high-frequency dynamics of HRV, (Malik et al., 1996). We calculated low-frequency (0.05 – 0.15 Hz; LF-HRV) and high-frequency (0.15-0.4 Hz; HF-HRV) power. Segments classified as atrial fibrillation were excluded from further analysis, and any participant with >50% atrial fibrillation was excluded.

2.5.2. *White matter hyperintensities (WMH)*

Estimates of white matter lesion burden in our sample have been reported previously (Fuhrmann et al., 2017). In summary, white matter lesion was estimated using the lesion growth algorithm in the LST toolbox for SPM (Schmidt et al., 2012) with κ of 0.7.

2.5.3. *Other risk factors of cardiovascular health: blood pressure and body mass index*

Systolic and diastolic blood pressure were measured at rest, seated, using an automated sphygmomanometer (A&D Medical Digital Blood Pressure Monitor, UA-774). The average of three measurements was used. BMI was calculated as weight (kg) / height (m)², using portable scales (Seca 875).

2.6. Data reduction

Datasets of interest stemmed from a wide range of modalities (RSFA, ASL, T1-weighted, FLAIR and ECG measures). To make these datasets tractable, we analysed a set of summary measures for each of the modality (also known as features or components) as illustrated in Figure 1. This had two advantages. First, it reduced the number of statistical comparisons. Second, it separated spatially overlapping sources of signal with different aetiologies within a modality (Xu et al., 2013), e.g. cardiovascular *versus* cerebrovascular signals, which may vary across individuals and brain region in RSFA (Tsvetanov et al., 2015) and ASL data (Mutsaerts et al., 2017). We used independent component analysis (ICA) across participants to derive spatial patterns of each imaging modality across voxels. As a proxy of vascular health, we used exploratory factory analysis to derive a latent variables from a set of measures related to cardiac function derived from the resting heart rate signal and other risk factors (Varadhan et al., 2009; Wardlaw et al., 2014).

2.6.1. *Indices of RSFA, T1 and CBF maps using Independent Component Analysis*

Group ICA was implemented on RSFA, GMV and CBF maps separately. For each modality, data were decomposed to a set of spatially independent sources using the Source Based Morphometry toolbox (Xu et al., 2009) in the Group ICA for fMRI Toolbox (GIFT; <http://mialab.mrn.org/software/gift>).

In brief, the fastICA algorithm was applied after the optimal number of sources explaining the variance in the data was identified using PCA with Minimum Description Length (MDL) criterion (Hui et al., 2011; Li et al., 2007; Rissanen, 1978). By combining the PCA and ICA, one can decompose an n-by-m matrix of participants-by-voxels into a source matrix that maps independent components (ICs) to voxels (here referred to as “IC maps”), and a mixing matrix that maps ICs to participants. The mixing matrix indicates the degree to which a participant expresses a defined IC. The loading values in the mixing matrix were scaled to standardized values (Z-scores) and used for between-participant analysis of summary measures from other modalities. The maximum number of available datasets within each modality was used, recognising that ICA decomposition accurately represents individual variation despite different group sizes while maximizing statistical power (Calhoun et al., 2008; Erhardt et al., 2011).

2.6.2. *Indices of vascular health using Exploratory Factor Analysis*

As a vascular health index, we sought a summary measure that characterized the complexity of cardiovascular signal (Varadhan et al., 2009; Wardlaw et al., 2014). We used factor analysis on the mean HR, high-frequency and low-frequency HRV, systolic and diastolic blood pressure, white matter hyperintensities and body-mass index to extract a set of latent variables reflecting variability in cardiovascular health across all individuals. The analysis used matlab *factoran.m* with default settings. Input variable distributions which deviated from Gaussian normality (1-sample Kolmogorov-Smirnov Test, p-value<0.05) were log-transformed (1-sample Kolmogorov-Smirnov Test, p-value > 0.05) (Fink, 2009).

2.7. Analytical approach

We performed both voxel-wise and component-based analyses using multiple linear regression (MLR) with robust fitting algorithm (matlab function *fitlm.m*). Voxel-level analysis was based on voxel-wise estimates across all imaging maps (RSFA, GM and ASL), while component-based analysis was based on component-wise estimates across all imaging components. We adopted a two-stage procedure for

each RSFA voxel/component (Figure 1). In the first stage we used MLR with RSFA values for all individuals as dependent variable. The second stage correlated the residuals from each model with age.

In the first level models, independent variables included either cardiovascular health, CBF or grey matter measures and RSFA values as dependent variable. Covariates of no interest included gender, head motion and handedness. In the model with grey matter (model V, see below), the signal defined in the CSF mask was considered as a covariate of no interest to minimize the influence of non-morphological confounds in T1-weighted data (Bhogal et al., 2017; Ge et al., 2017; Tardif et al., 2017). Additional inclusion of total intracranial volume (TIV) did not change the principal results. Non-normally distributed variables were logarithmically or exponentially transformed to conform normality (Fink, 2009).

We constructed five models:

- Model 1: Covariates [of no interest]

$$y \sim \beta_0 1 + Covs + \varepsilon$$

- Model 2: Covariates and cerebrovascular measures

$$y \sim \beta_0 1 + \beta_1 CBF_1 + Covs + \varepsilon_{CBF}$$

- Model 3: Covariates and cardiovascular measures

$$y \sim \beta_0 1 + \beta_1 CVH + Covs + \varepsilon_{CVH}$$

- Model 4: Covariates, cardiovascular and cerebrovascular measures

$$y \sim \beta_0 1 + \beta_1 CBF + \beta_2 CVH + Covs + \varepsilon_{CBF,CVH}$$

- Model 5: Covariates and grey matter volume measures

$$y \sim \beta_0 1 + \beta_1 GMV + Covs + \varepsilon_{GMV}$$

Note that the independent variables in Models 2, 4 and 5 included measures with voxel-specific information, i.e. RSFA values across subjects in a given voxel were predicted by the CBF/GM values for the corresponding voxel.

The residuals, ϵ , from each model were then used in a second-stage linear regression (i.e. correlational analysis) to estimate their association with age. Voxels where the residuals correlate with age ($p < .05$, FDR-corrected) indicate that the independent variables in first-stage model could not explain sufficiently the age-dependent variability in RSFA. Conversely, residuals not associated with age would suggest that the independent variables considered in the model are sufficient to explain age-dependent variability in RSFA.

This two-stage procedure was performed for each voxel of RSFA maps resulting in a statistics map for each model indicating the association between residuals and age. Statistical maps were corrected for multiple comparisons at $p < 0.05$ (FDR-corrected). To further address multiple comparisons and voxel-voxel mapping between modalities, we performed complementary analysis where voxel-wise estimates of brain measures were substituted with subject-wise IC loadings, see Section 2.6.

We also tested whether the distribution of age-RSFA residuals correlations across all voxels formed differed from the predicted distribution under pure randomness. We constructed 5000 distributions of age-RSFA residual correlations across all brain voxels (D_{Voxels}), where RSFA residuals were based either on a model with observed RSFA values ($D_{\text{Voxels}1}$) or permuted RSFA values ($D_{\text{Voxels}2-5000}$). Distribution medians and distribution shapes were compared using Wilcoxon rank sum test and Kolmogorov-Smirnov test respectively. We performed a pair-wise comparison across all 5000 distribution shapes using Kolmogorov-Smirnov test, resulting in a distribution of 4999 similarity scores ($D_{\text{Similarity}}$) between each D_{Voxels} with the remaining 4999 D_{Voxels} . Next, we estimated the number of times (N_p) the distribution of similarity for observed RSFA values ($D_{\text{Similarity}1}$) is statistically different than the permuted distributions of similarities ($D_{\text{Similarity}2-5000}$) using Wilcoxon rank sum test. The ratio $N_p/5000$ provided a level of significance, e.g. a value < 0.05 suggested that the distribution of age-RSFA residual values is not as predicted by a model with pure randomness (at significance level $p < 0.05$) and suggests an association between age and RSFA residuals. The procedure was applied separately for each of the

five models across all brain voxels, as well as for different tissue types (cerebrospinal fluid, grey matter and white matter voxels with values above 0.4 in SPM's tissue probability maps).

3. Results

3.1. Main and age effects of RSFA, CBF and CVH

3.1.1. *Resting state fluctuation amplitudes (RSFA)*

Whole group voxel-wise analysis revealed relatively high RSFA values (relative to the average across the brain) across all individuals in the frontal orbital, inferior frontal gyrus (IFG), dorsolateral prefrontal cortex (dlPFC), superior frontal cortex, anterior and posterior cingulate, and lateral parietal cortex (Figure 2a). With respect to aging, we observed age-related decreases in RSFA in the bilateral IFG, bilateral dlPFC, bilateral superior frontal gyrus, primary visual cortex, cuneus, precuneus, posterior and anterior cingulate, superior temporal gyrus, medial parietal cortex, and lateral parietal cortex (Figure 2b). Regions in the proximity of frontal white matter, cerebrospinal fluid and large vascular vessels showed a significant increase of RSFA values as a function of age.

3.1.2. *Cerebral blood flow (CBF)*

Whole group voxel-wise analysis revealed a pattern of relatively high cerebral blood flow across all individuals in cortical and subcortical brain areas with high perfusion and metabolism properties (Figure 2c) including caudal middle-frontal, posterior cingulate, pericalcarine, superior temporal and thalamic regions. Moderate to low CBF values in the superior-parietal and inferior-frontal areas of the cortex (Figure 2c, every 10 axial slices from -30 to 70) may reflect the axial positioning of the partial brain coverage sequence used in the study. With respect to aging, we observed age-related reductions in CBF in the bilateral dorsolateral prefrontal cortex, lateral parietal cortex, anterior and posterior cingulate, pericalcarine and cerebellum (Figure 2c). In addition, we observed age-related CBF increase in regions susceptible to individual and group differences in arterial transit time biasing the accuracy of CBF estimation, including middle temporal gyrus (Mutsaerts et al., 2017).

3.1.3. Grey matter volume (GMV)

We identified significant whole-group effects across all grey matter voxels (Figure 2e). In addition, there was a widespread age-related decrease in GMV, in bilateral temporal lobes, bilateral prefrontal, middle and superior frontal areas, bilateral medial occipital areas, cerebellum, and subcortical areas including thalamus, caudate and putamen (Figure 2f), consistent with previous reports (Mohajer et al., 2020; Peelle et al., 2012; Tsvetanov et al., 2019).

3.1.4. Cardiovascular health (CVH)

An exploratory factor analysis with principal component analysis indicated a three-factor structure of the cardiovascular health and risk measures. Factor 1 loadings indicated a factor expressing variability in blood pressure measures, where individuals with higher subject scores had larger systolic and diastolic pressure (Figure 3). Subjects scores did not correlate with age ($r = +.061$, $p=.328$), indicating that variability in blood pressure was not associated uniquely with aging over and above their contribution to other factors in the analysis. Factor 2 was mainly expressed by heart rate and HRV measures, where individuals with high subject scores had low resting pulse and high HRV metrics. Subject scores were correlated negatively with increasing age ($r = -.417$, $p<.001$), consistent with findings of age-related decrease in HRV (Figure 3). Finally, Factor 3 was expressed negatively by HRV and positively by WMH and systolic blood pressure, indicating that individuals with high subjects scores were more likely to have high burden of WMH, high systolic blood pressure and low HRV (Figure 3). Subject scores were associated positively with age ($r = +.713$, $p<.001$), suggesting that a portion of the age-related decrease in HRV is coupled with increase in WMH and systolic blood pressure.

3.2. Correlations between Age and RSFA residuals

3.2.1. Voxel-based analysis

Covariates of no interest only (Model I)

The whole-group voxel-wise analysis of RSFA maps revealed brain regions with high vascular reactivity including frontal orbital, inferior frontal gyrus, inferior frontal gyrus, dorsolateral prefrontal

cortex, superior frontal cortex, anterior and posterior cingulate, and lateral parietal cortex. We observed age-related decrease in RSFA in the bilateral inferior frontal gyrus, bilateral dorsolateral prefrontal cortex, bilateral superior frontal gyrus, primary visual cortex, cuneus, precuneus, posterior and anterior cingulate, superior temporal gyrus, medial parietal cortex, and lateral parietal cortex. In addition, we observed age-related decrease in RSFA in the proximity of ventricles and large vascular vessels.

Controlling for Cerebrovascular Factors (Model II)

We observed significant correlations between age and the RSFA residuals after controlling for subject variability in CBF and covariates of no interest at an FDR-adjusted p-value of 0.05 (Figure 4, model II). The spatial extent and the size of the statistical maps were similar to the analysis with RSFA residuals after controlling for covariates only (Figure 2d and Figure 4, model I), suggesting that CBF does not fully explain variability in RSFA.

Controlling for Cardiovascular Factors (Model III)

We observed no significant correlations between age and the RSFA residuals after controlling for variability in CVH and covariates of no interest at an FDR-adjusted p-value of 0.05 (Figure 4, model III), suggesting that CVH can explain sufficiently age-dependent variability in RSFA, at least at the level of statistically-corrected voxels.

Controlling for Cardiovascular and Cerebrovascular Factors (Model IV)

We observed no significant correlations between age and the RSFA residuals after controlling for variability in CVH, CBF and covariates of no interest at an FDR-adjusted p-value of 0.05 (Figure 4, model IV), suggesting that CVH and CBF together explain sufficiently age-dependent variability in RSFA.

Controlling for Grey Matter Volume (Model V)

We observed significant correlations between age and the RSFA residuals after controlling for grey matter volume (GMV) and covariates of no interest at an FDR-adjusted p-value of 0.05 (Figure 4, model V), suggesting that GMV does not adequately explain variability in RSFA, at the voxel-wise level.

3.2.2. *Distribution-based analysis*

The medians of observed and permuted data did not differ significantly ($p > .1$ for all five models). In terms of the distributions, the level of statistical significance decreased after controlling for cardiovascular, cerebrovascular and GMV signals ($p < .001$, $p < .001$, $p = .015$, and $p < .001$ for models 1, 2, 3 and 5 respectively), see Table 2. The model considering jointly cardiovascular and cerebrovascular signals (model 4) indicated a difference in the distribution of observed and permuted data ($p = 0.016$), reflecting a small level of correlation between age and RSFA residuals in some voxels. It is unclear whether the signal originated in a particular tissue type, so we repeated the permutation approach for each tissue type separately (Table 2). For models 1, 2 and 5 the RSFA residuals were associated with age across all three tissue types, suggesting that variability in cerebrovascular and grey matter cannot account fully for the effects of age on RSFA in all tissue types. However, the models controlling for cardiovascular health (Models 3 and 4) were not significant for grey matter and white matter tissue. The analysis on CSF voxels was highly significant suggesting that any potential age-related effects on RSFA not captured by cardiovascular and cerebrovascular signals on voxel-level are focal to CSF areas, rather than grey matter or white matter.

3.2.3. *Component-based analysis*

CVH signals sufficiently explained variance in RSFA, in the voxel-based analysis (after FDR correction for multiple comparisons) and in grey-matter areas in distribution-based analysis. This was not the case for CBF or GMV in the voxel-based analysis, as well as for CVH in CSF regions in distribution-based analysis. However, this might reflect limitations of these analyses to separate spatially overlapping sources of signal with different aetiology and the large number of comparisons (see Methods). Therefore, we used independent component analysis to decompose each imaging modality to a small number of spatially-independent components and test their ability to explain variance of RSFA.

Figure 5 shows the decomposition of the RSFA, CBF and GMV datasets with 18, 13 and 16 number of components, respectively, according to the MDL criterion (Li et al., 2007). The spatial maps of the components and the between subject-correlations of loading values revealed patterns of signal from grey matter, white matter, cerebrospinal fluid and vascular aetiology (Figure 5), which were highly consistent with voxel-wise analysis (Figure 2), previous reports of RSFA (Tsvetanov et al., 2015) and structural data (Eckert et al., 2010; K. Liu et al., 2017).

The effects of ageing on the independent components loadings was consistent with the voxel-level analysis. Specifically, RSFA components with vascular ethology indicated an age-related increase in the loading values, while ICs confined within grey matter areas showed age-related decrease in the loading values (Figure 5a, left side of the panel). Several CBF components demonstrated age-related decrease in loading values, including inferior frontal gyrus, superior frontal gyrus, cuneus, precuneus, lateral occipital cortex and motor cortex (Figure 5b, left side of the panel). All but one GMV component in the cerebellum demonstrated age-related decrease in loading values consistent with brain-wide atrophy in ageing (Figure 5).

Next, we turn to the correlations between age and residuals of the RSFA ICs. We focused on ICs that showed age-related differences in the subject loading values (10 out of 18), after controlling for CBF IC loading values, GMV IC loading values or CVH factor loadings (Figure 6).

Controlling for Cerebrovascular Factors (Model II)

The associations between age and RSFA residuals after controlling for CBF loading values were weaker in vascular ICs and abolished in GM ICs compared to the analysis with covariates only (Figure 6, Model I vs Model 2). Unlike in the voxel-based analysis, this ICA approach suggests that CBF does explain some age-related variability in RSFA across many networks, especially those in GM areas, which may be due to reduced number of comparisons and improved characterisation of sources of signals in RSFA and CBF data using ICA.

Controlling for Cardiovascular Factors (Model III)

After controlling for differences in CVH, RSFA residuals in two ICs (IC3 and IC7) were correlated with age (uncorrected p-value at 0.05 significance level), although to a lesser extent compared to the analysis with covariates only (Model III vs Model I), indicating that CVH can explain age-dependent variability in most, but not all, RSFA ICs.

Controlling for Cerebrovascular and Cardiovascular Factors (Model IV)

We observed no significant correlations between age and the RSFA residuals after controlling for variability in CVH and CBF (even at an uncorrected p-value of 0.05, see Figure 6), suggesting that together, CVH and CBF can explain age-dependent variability in RSFA.

Controlling for Grey Matter Volume (Model V)

RSFA ICs adjusted for GMV ICs demonstrated reduced correlations between RSFA and age (particularly RSFA ICs of grey matter territories), indicating that age-related differences in RSFA ICs can be partly explained by grey matter atrophy.

Controlling for Grey Matter Volume independent of Cardiovascular Factors

Some degree of association between age differences in RSFA and grey matter atrophy is expected given cardiovascular health has been linked to brain-wide atrophy (Gu et al., 2019; Srinivasa et al., 2016) and T1-weighted data is confounded by non-morphological signals (Bhogal et al., 2017; Ge et al., 2017; Tardif et al., 2017). Therefore, to test whether the effects of brain atrophy on RSFA were independent of the effects of CVH on brain atrophy, we controlled for the effects of CVH in GMV ICs. Then we used the GMV residuals after fitting CVH to GMV IC loadings (i.e. GMV orthogonalised with respect to CVH) to estimate RSFA residuals and subsequently their correlation with age (Figure 6, Model 6). The effects between RSFA residuals and age in Model 6 were similar to Model 1, suggesting that GMV differences independent of CVH were not correlated to differences in RSFA.

394

395 4. Discussion

396 The principle result of this study is to confirm the suitability of resting state fluctuation amplitude (RSFA)
397 to quantify vascular influences in BOLD-based fMRI signals, and to demonstrate that the age effects on
398 RSFA reflect variability in vascular factors rather than neuronal factors. We demonstrate that the effects
399 of age on RSFA can be sufficiently captured by the joint consideration of cardiovascular (based on ECG,
400 BP, WMH and BMI measures) and cerebrovascular factors (CBF from ASL). Variance in brain atrophy
401 (GM volume Figure 6) and neuronal activity (Kumral et al., 2019; Tsvetanov et al., 2015) do not explain
402 unique relationship between RSFA and age. This means that RSFA is a suitable measure for
403 differentiating between vascular and neuronal influences on task-based BOLD signal. Without
404 modelling the age-related differences in cardiovascular and cerebrovascular factors, changes in
405 'activity' based on BOLD-fMRI could be misinterpreted, thereby undermining conceptual advances in
406 cognitive ageing.

407 Cardiovascular factors and age-differences in RSFA

408 We used factor analysis to estimate cardiovascular health from a wide range of cardiovascular
409 measures (Varadhan et al., 2009; Wardlaw et al., 2014). Our three factor solution resembled previous
410 reports (Chen et al., 2000; Goodman et al., 2005; Khader et al., 2011; Mayer-Davis et al., 2009), with
411 two factors associated with blood pressure and heart rate variability (factors 1 and 2, respectively). A
412 third factor expressed white matter hyperintensities, blood pressure, heart rate variability and body-
413 mass index, suggesting a cerebrovascular origin.

414 These three factor indices of cardiovascular health explained most of the age-related variability
415 in RSFA, leaving little to no associations between age and RSFA residuals in grey matter regions (after
416 controlling for these cardiovascular signals). This suggests that differences in cardiovascular health
417 mediate most of the age effects on RSFA (Tsvetanov et al., 2015). Interestingly, each CVH factor was

associated with a distinct spatial RSFA pattern (Supplementary Figure 2) and collectively provided additional explanatory value for the overall age-differences in brain-wide RSFA. Next, we turn to neural and cerebrovascular contributions to BOLD.

Cerebrovascular signals and age-differences in RSFA

Our measure of cerebrovascular function was based on cerebral blood flow estimates from a common perfusion-based ASL sequence. Here, we refer to cerebrovascular function as an umbrella term of physiological alterations in the neurovascular unit including resting CBF, cerebrovascular reactivity, cerebral autoregulation and pulsatility. The observed average, gender and age effects were consistent with previous reports. The age effects on CBF values were in agreement with previous reports (Chen et al., 2011; Zhang et al., 2018), with decreases mainly found in regions that are associated with high perfusion and metabolic demand, including precuneus, cuneus, prefrontal cortices and cerebellum. The mechanisms underlying the observed CBF decrease across the adult lifespan is a subject of continuous debate between structural and physiological alterations of the neurovascular unit (Girouard and Iadecola, 2006; Tarumi and Zhang, 2018; Tsvetanov et al., 2020). We also observed age-related increase in CBF in temporal regions, which may reflect macro-vascular artifacts that are common to arterial spin labelling findings (Detre et al., 2012; Mutsaerts et al., 2017) due to prolonged arterial transit time with ageing (Dai et al., 2017). This nonspecific nature of resting CBF signal changes during ageing is particularly problematic for fMRI BOLD studies, since differences in physiology on that level may confound the interpretation of the BOLD signal as a surrogate measure of evoked neural activity (Whittaker et al., 2016).

Compared to voxel-wise estimates, our component-wise CBF values captured better the age-related effects of RSFA, especially in grey matter areas (see below on differences between voxel-wise and component-wise analysis). Nevertheless, neither the voxel-wise nor component-based analysis of CBF values could explain sufficiently the effects of age on RSFA, suggesting that RSFA may not be attributed exclusively to sources of signal linked to cerebrovascular function (Garrett et al., 2017; Liu et

al., 2012). There was a positive correlation between resting CBF and RSFA in brain areas typically associated with high blood perfusion and metabolic demands, including cuneus, precuneus, intraparietal sulcus, inferior temporal cortices, dorsolateral prefrontal cortex and anterior cingulate (Supplementary Figure 3). But, we also observed negative associations between RSFA and CBF in inferior brain areas, mainly close to vascular territories i.e. the higher the RSFA the lower the CBF values were in these regions (Supplementary Figure 3). This may reflect the dominance of pulsatility influences in RSFA signals near vascular territories and the CSF (for more information see section: Spatial distribution and age effects on RSFA). This may have adverse effects on tissue perfusion in neighboring areas (Tarumi et al., 2014). The coexistence between positive and negative relationships between RSFA and CBF measures in our study explains previous observations of a varied direction in the relationship between these measures across regions for groups and individuals with differences in vascular health (Garrett et al., 2017).

Joint effect of cardiovascular and cerebrovascular factors

The joint consideration of cardiovascular and CBF measures fully explained the (significant) effects of age on RSFA in grey matter regions, despite their differential association with ageing (Zlokovic, 2011). This suggests that RSFA can normalize BOLD fMRI for both cardiovascular and cerebrovascular factors as highly reliable and temporally stable measurement compared to current standard approaches to normalize BOLD fMRI (eg. hypercapnia) (Golestani et al., 2015; Lipp et al., 2015). Lower reproducibility in “gold standard” approaches could be due to susceptibility of cerebrovascular measures to short-term variable physiological modifiers (e.g. caffeine, nicotine, time of the day, drowsiness) (Clement et al., 2018). The high reproducibility of RSFA in healthy adults could come from the additional contribution of short-term but stable cardiovascular health signals (e.g. heart condition or white matter hyperintensities), which are independent of cerebrovascular factors. RSFA reflects both cardiovascular and cerebrovascular signals, which are associated with distinct spatial patterns (see section Spatial distribution and age effects on RSFA). RSFA can help dissociate age-related differences

in cardiovascular, cerebrovascular and neural function in task-based BOLD signal, which is important for using fMRI to understand the mechanisms of cognitive aging.

Grey matter volume and age-differences on RSFA

Voxel-wise and component-based analyses indicated weak associations between age-differences in RSFA and grey matter volume, which were abolished after adjusting for variability in cardiovascular health. Interestingly, the strongest effects were at the boundaries between grey matter and other tissue types (white matter and CSF), rather than deep cortical areas (Supplementary Figure 3). The spatial pattern of the effects for cortical areas was similar to those observed between CBF and RSFA measures. There was a positive relationship between RSFA and grey matter volume in the precuneus, intraparietal sulcus, dorsolateral prefrontal cortex and dorsal anterior cingulate; which could reflect the cerebrovascular component of the RSFA signal (see above). In addition, the cerebellum and subcortical areas near vascular territories showed negative associations, i.e. individuals with less grey matter volume had larger RSFA values, likely reflecting the cardiovascular components of the RSFA signal (see below, Spatial distribution and age effects of RSFA). Importantly, there were no associations between RSFA and grey matter volume after adjusting for cardiovascular health. This is suggestive of an indirect association between RSFA and grey matter volume introduced by cardiovascular effects on brain-wide atrophy (Gu et al., 2019; Srinivasa et al., 2016) and other non-morphological confounds in T1-weighted data (Bhogal et al., 2017; Ge et al., 2017; Tardif et al., 2017). The lack of evidence for an association between age-related effects on RSFA and brain atrophy after adjusting for cardiovascular health is consistent with previous reports using direct physiological measures of neural activity (MEG and EEG): no age-related associations between RSFA and neuronal indices were detected (Kumral et al., 2019; Tsvetanov et al., 2015). Furthermore, potential age-related associations between RSFA and cognitive function are fully explained by cerebrovascular risk factors, such as WMH burden (Millar et al., 2020). Taken together these findings suggest that the age-related differences in BOLD signal variability at resting state are unlikely to be of neuronal origin beyond the effects of age on various types of vascular signals.

494

495 Spatial distribution and age effects on RSFA

496 The voxel-wise and component-based analysis of RSFA maps reveal brain regions with high vascular
497 reactivity (Di et al., 2012; Kalcher et al., 2013; Kannurpatti et al., 2011; Liu et al., 2013; Mueller et al.,
498 2013; Yezhuvath et al., 2009), and accord with previous studies of average and age-effects on RSFA
499 (Golestani et al., 2016; Lipp et al., 2015; P. Liu et al., 2017; Tsvetanov et al., 2015). These patterns of
500 spatially distinct cortical areas might reflect segregation of cortical tissue composition, e.g. delineation
501 on the basis of vascular density and metabolic demands in areas with cyto- or myeloarchitectonic
502 differences (Annese et al., 2004; Fukunaga et al., 2010; Geyer et al., 2011; Glasser and Van Essen, 2011).
503 The age-related increase in RSFA in areas with vascular, WM and CSF partitions may reflect the impact
504 of vascular pulsatility downstream of cerebral arteries due to wall stiffening of blood vessels (Robertson
505 et al., 2010; Webb et al., 2012), which may influence BOLD signal variability in neighboring brain tissue
506 (Lee and Oh, 2010; O'Rourke and Hashimoto, 2007; Tarumi et al., 2014; Viessmann et al., 2017). The
507 pulsatility can influence signal in white matter and cerebrospinal fluid areas (Makedonov et al., 2013;
508 Tarumi et al., 2014; Theyers et al., 2018; Viessmann et al., 2019). In addition, it is also possible that the
509 RSFA signal in one area of the brain captures the presence of multiple sources of signal with different
510 aetiology. For example, the observed signal in one CSF voxel may be a mixture of signals coming from
511 fluctuations in resting CBF in neighboring vascular territories and pulsatility influences in the
512 perivascular space. Spatially overlapping sources of signal might be difficult to detect and dissociate
513 using a univariate approach. This motivates the use of multivariate data-driven approaches, as
514 highlighted by our findings. In sum, this suggests that RSFA reflects different types of vascular signals
515 with distinct spatial patterns in terms of signals with cerebrovascular origin in grey matter regions, and
516 those with cerebro- and cardio-vascular origin in other parts of the brain.

517

Limitations and future directions

There are limitations to the current study. In terms of cardiovascular health, there may be more important measures that were not present in the CamCAN sample. Moreover, the analysis of heart rate variability estimates was based on normal-to-normal beats (Vest et al., 2018). The difference between NN- and RR-beat analysis is that the former considers the detection and exclusion of segments and participants with atrial fibrillation and other abnormal beats. While NN-beat analysis optimises the detection of unbiased estimates of cardiovascular health, it also precludes sensitivity to potential effects of arrhythmia and abnormal heart beats on RSFA in our analysis, which might be relevant to regions susceptible to pulsatility effects (Webb and Rothwell, 2014).

In terms of cerebrovascular signals, the use of ASL-based CBF measurements could be complemented with individual-based arterial transit time measurement in order to improve the accuracy of ASL imaging in older populations (Dai et al., 2017). There are also other means to assess cerebrovascular function, including cerebrovascular reactivity, including CO₂-inhalation-induced hypercapnia (Liu et al., 2019), breath-hold-induced hypercapnia (Handwerker et al., 2007; Mayhew et al., 2010; Riecker et al., 2003; Thomason et al., 2007, 2005), hyperventilation-induced hypocapnia (Bright et al., 2009; Krainik et al., 2005), and venous oxygenation (Liau and Liu, 2009; Lu et al., 2010; Restom et al., 2007) and it is possible that these might reveal effects in RSFA where ASL-based CBF does not. Future studies should explore the utility of additional estimates from resting ASL-based CBF data to complement CBF quantification. For instance, little is known about whether resting CBF variability, which is statistically similar to RSFA, is sensitive to cerebrovascular reactivity and other vascular origins (Robertson et al., 2017). The ease, safety and tolerability of RSFA across the lifespan yields a considerable advantage for population and clinical studies.

Similar to the CBF analyses, the GMV findings generalized across voxel-wise and component-based analysis, but the component-based analysis seemed to be more sensitive to the age effects on RSFA in both CBF and GMV datasets. The greater generalization across datasets with independent component

analysis than voxel-based analysis may reflect several factors (Calhoun and Adali, 2008; Passamonti et al., 2019; Sui et al., 2012), e.g. reducing the burden of multiple comparisons, pooling information across multiple voxels with similar profiles, separating sources of signal with different etiology but with overlapping topologies and possibly improving the spatial correspondence across imaging modalities with different spatial scales, sequence parameters and signal properties. Therefore, the use of component-based analysis in studies comparing approaches for normalization of physiological signals may improve understanding the nature of the signal and the extent to which these neuroimaging modalities are related to one another.

In the current study, RSFA was estimated from resting state fMRI BOLD data prior to collection of other task-based fMRI scanning as in previous validation studies of RSFA (Kannurpatti and Biswal, 2008; Tsvetanov et al., 2015). Other means of RSFA-like estimates have been proposed for scaling BOLD activation data using fMRI BOLD data at different non-resting cognitive states, e.g. during task periods (Kazan et al., 2016) or fixation-/resting-periods succeeding task periods (Garrett et al., 2017). Given that short periods of cognitive engagement can modulate the BOLD signal in a subsequent resting state scan (Sami et al., 2014; Sami and Miall, 2013), future studies are required to generalise our findings to RSFA-like estimates derived from other types of fMRI BOLD acquisition.

Finally, this study has focussed on the effects of aging, but other studies aiming to understand individual differences or drug effects in fMRI BOLD might be affected in a similar manner. Therefore, future studies should consider the origins of the signal contributing to RSFA (cerebrovascular vs cerebrovascular) and more broadly their influence in fMRI BOLD imaging studies. In the light of increasing evidence of the role of cardiovascular and cerebrovascular factors in maintaining cognitive function, future studies might even consider RSFA as a predictor, rather than just as a covariate of no interest, when modelling the effects of interest (e.g. age or performance). Furthermore, while the proposed approach is based on plausible neurophysiology that can be used to evaluate its contribution to cognitive function, future studies could improve absolute quantification of neural function together

with its integration with deoxyhaemoglobin-dilution-based modelling (Davis et al., 1998; Hoge et al., 1999a, 1999b), haemodynamic response function modelling (West et al., 2019), generative modelling (Friston et al., 2003; Jafarian et al., 2020; Tsvetanov et al., 2016) and model-free decomposition (Bethlehem et al., 2020; Campbell et al., 2015; Samu et al., 2017; Tsvetanov et al., 2018) of fMRI BOLD data.

Concluding remarks

Cardiovascular and cerebrovascular signals together predict the age differences in RSFA, establishing RSFA as an important marker that can be used to accurately separate vascular signals from neuronal signals in the context of BOLD fMRI. We propose that RSFA is suitable to normalize BOLD, and control for differences in cardiovascular signals. This is particularly relevant to the research in neurocognitive aging, and may reduce selection bias, for example by permitting the inclusion of individuals with a wider range of hypertension, cardiovascular conditions or comorbidity. The use of RSFA as a mechanism to adjust for confounds in BOLD-fMRI, or as a predictor, will allow the development of better models of ageing and age-related disorders (Cabeza et al., 2018; Tsvetanov et al., 2018).

5. Acknowledgements

This work is supported by the British Academy (PF160048), the Guarantors of Brain (101149), the Wellcome Trust (103838), the Medical Research Council (SUAG/051 G101400; and SUAG/046 G101400), European Union's Horizon 2020 (732592) and the Cambridge NIHR Biomedical Research Centre.

6. References

- Annese, J., Pitiot, a., Dinov, I.D.D., Toga, a. W.W., 2004. A myelo-architectonic method for the structural classification of cortical areas. *Neuroimage* 21, 15–26. <https://doi.org/10.1016/j.neuroimage.2003.08.024>
- Ashburner, J., 2007. A fast diffeomorphic image registration algorithm. *Neuroimage* 38, 95–113. <https://doi.org/10.1016/j.neuroimage.2007.07.007>
- Ashburner, J., Friston, K.J., 2005. Unified segmentation. *Neuroimage* 26, 839–51. <https://doi.org/10.1016/j.neuroimage.2005.02.018>
- Beard, J.R., Officer, A., de Carvalho, I.A., Sadana, R., Pot, A.M., Michel, J.-P., Lloyd-Sherlock, P., Epping-Jordan, J.E., Peeters, G.M.E.E. (Geeske), Mahanani, W.R., Thiyagarajan, J.A., Chatterji, S., 2016. The World report on ageing and health: a policy framework for healthy ageing. *Lancet* 387, 2145–2154. [https://doi.org/10.1016/S0140-6736\(15\)00516-4](https://doi.org/10.1016/S0140-6736(15)00516-4)
- Bethlehem, R.A.I., Paquola, C., Seidlitz, J., Ronan, L., Bernhardt, B., Cam-CAN, Tsvetanov, K.A., 2020. Dispersion of functional gradients across the lifespan. *bioRxiv* 2020.02.27.968537. <https://doi.org/10.1101/2020.02.27.968537>
- Bhagal, A.A., Siero, J.C., Zwanenburg, J., Luijten, P.R., Philippens, M.E., Hoogduin, H., 2017. Quantitative T1 mapping under precisely controlled graded hyperoxia at 7T. *J. Cereb. Blood Flow Metab.* 37, 1461–1469. <https://doi.org/10.1177/0271678X16656864>
- Bright, M.G., Bulte, D.P., Jezzard, P., Duyn, J.H., 2009. Characterization of regional heterogeneity in cerebrovascular reactivity dynamics using novel hypocapnia task and BOLD fMRI. *Neuroimage* 48, 166–75. <https://doi.org/10.1016/j.neuroimage.2009.05.026>
- Cabeza, R., Albert, M., Belleville, S., Craik, F.I.M., Duarte, A., Grady, C.L., Lindenberger, U., Nyberg, L., Park, D.C., Reuter-Lorenz, P.A., Rugg, M.D., Steffener, J., Rajah, M.N., 2018. Maintenance, reserve and compensation: the cognitive neuroscience of healthy ageing. *Nat. Rev. Neurosci.* 19, 701–710. <https://doi.org/10.1038/s41583-018-0068-2>
- Calhoun, V.D., Adali, T., 2008. ICA for Fusion of Brain Imaging Data, in: *Signal Processing Techniques for Knowledge Extraction and Information Fusion*. Springer US, Boston, MA, pp. 221–240. https://doi.org/10.1007/978-0-387-74367-7_12
- Calhoun, V.D., Maciejewski, P.K., Pearlson, G.D., Kiehl, K.A., 2008. Temporal lobe and “default” hemodynamic brain modes discriminate between schizophrenia and bipolar disorder. *Hum. Brain Mapp.* 29, 1265–1275. <https://doi.org/10.1002/hbm.20463>
- Campbell, K.L., Shafto, M.A., Wright, P., Tsvetanov, K.A., Geerligs, L., Cusack, R., Tyler, L.K.L.K., Brayne, C., Bullmore, E.E., Calder, A., Dalgleish, T., Duncan, J., Henson, R., Matthews, F., Marslen-Wilson, W., Rowe, J., Cheung, T., Davis, S., Kievit, R., McCarrey, A., Price, D., Taylor, J., Williams, N., Bates, L., Emery, T., Erzinçlioglu, S., Gadie, A., Gerbase, S., Georgieva, S., Hanley, C., Parkin, B., Troy, D., Allen, J., Amery, G., Amunts, L., Barcroft, A., Castle, A., Dias, C., Dowrick, J., Fair, M., Fisher, H., Goulding, A., Grewal, A., Hale, G., Hilton, A., Johnson, F., Johnston, P., Kavanagh-Williamson, T., Kwasniewska, M., McMinn, A., Norman, K., Penrose, J., Roby, F., Rowland, D., Sargeant, J., Squire, M., Stevens, B., Stoddart, A., Stone, C., Thompson, T., Yazlik, O., Dixon, M., Barnes, D., Hillman, J., Mitchell, J., Willis, L., 2015. Idiosyncratic responding during movie-watching predicted by age differences in attentional control. *Neurobiol. Aging* 36, 3045–3055. <https://doi.org/10.1016/j.neurobiolaging.2015.07.028>
- Chang, C., Cunningham, J.P., Glover, G.H., 2009. Influence of heart rate on the BOLD signal: the cardiac

630 response function. *Neuroimage* 44, 857–69. <https://doi.org/10.1016/j.neuroimage.2008.09.029>

631 Chang, C., Metzger, C.D., Glover, G.H., Duyn, J.H., Heinze, H.-J., Walter, M., 2013. Association between
632 heart rate variability and fluctuations in resting-state functional connectivity. *Neuroimage* 68, 93–
633 104. <https://doi.org/10.1016/j.neuroimage.2012.11.038>

634 Chen, J.J., Rosas, H.D., Salat, D.H., 2011. Age-associated reductions in cerebral blood flow are
635 independent from regional atrophy. *Neuroimage* 55, 468–78.
636 <https://doi.org/10.1016/j.neuroimage.2010.12.032>

637 Chen, W., Bao, W., Begum, S., Elkasabany, A., Srinivasan, S.R., Berenson, G.S., 2000. Age-related
638 patterns of the clustering of cardiovascular risk variables of syndrome X from childhood to young
639 adulthood in a population made up of black and white subjects: the Bogalusa Heart Study.
640 *Diabetes* 49, 1042–8. <https://doi.org/10.2337/diabetes.49.6.1042>

641 Clement, P., Mutsaerts, H.-J., Václavů, L., Ghariq, E., Pizzini, F.B., Smits, M., Acou, M., Jovicich, J.,
642 Vanninen, R., Kononen, M., Wiest, R., Rostrup, E., Bastos-Leite, A.J., Larsson, E.-M., Achten, E.,
643 2018. Variability of physiological brain perfusion in healthy subjects – A systematic review of
644 modifiers. Considerations for multi-center ASL studies. *J. Cereb. Blood Flow Metab.* 38, 1418–
645 1437. <https://doi.org/10.1177/0271678X17702156>

646 Cusack, R., Vicente-Grabovetsky, A., Mitchell, D.J., Wild, C.J., Auer, T., Linke, A.C., Peelle, J.E., 2014.
647 Automatic analysis (aa): efficient neuroimaging workflows and parallel processing using Matlab
648 and XML. *Front. Neuroinform.* 8, 90. <https://doi.org/10.3389/fninf.2014.00090>

649 Dai, W., Fong, T., Jones, R.N., Marcantonio, E., Schmitt, E., Inouye, S.K., Alsop, D.C., 2017. Effects of
650 arterial transit delay on cerebral blood flow quantification using arterial spin labeling in an elderly
651 cohort. *J. Magn. Reson. Imaging* 45, 472–481. <https://doi.org/10.1002/jmri.25367>

652 Davis, T.L., Kwong, K.K., Weisskoff, R.M., Rosen, B.R., 1998. Calibrated functional MRI: Mapping the
653 dynamics of oxidative metabolism. *Proc. Natl. Acad. Sci. U. S. A.* 95, 1834–1839.
654 <https://doi.org/10.1073/pnas.95.4.1834>

655 Detre, J.A., Rao, H., Wang, D.J.J., Chen, Y.F., Wang, Z., 2012. Applications of arterial spin labeled MRI in
656 the brain. *J. Magn. Reson. Imaging* 35, 1026–1037. <https://doi.org/10.1002/jmri.23581>

657 Di, X., Kannurpatti, S.S., Rypma, B., Biswal, B.B., 2012. Calibrating BOLD fMRI Activations with
658 Neurovascular and Anatomical Constraints. *Cereb. cortex* 1817, 1–9.
659 <https://doi.org/10.1093/cercor/bhs001>

660 Eckert, M.A., Keren, N.I., Roberts, D.R., Calhoun, V.D., Harris, K.C., 2010. Age-related changes in
661 processing speed: unique contributions of cerebellar and prefrontal cortex. *Front. Hum. Neurosci.*
662 4, 10. <https://doi.org/10.3389/neuro.09.010.2010>

663 Erhardt, E.B., Rachakonda, S., Bedrick, E.J., Allen, E.A., Adali, T., Calhoun, V.D., 2011. Comparison of
664 multi-subject ICA methods for analysis of fMRI data. *Hum. Brain Mapp.* 32, 2075–2095.
665 <https://doi.org/10.1002/hbm.21170>

666 Fink, E.L., 2009. The FAQs on Data Transformation. *Commun. Monogr.* 76, 379–397.
667 <https://doi.org/10.1080/03637750903310352>

668 Folstein, M.F., Folstein, S.E., McHugh, P.R., 1975. “Mini-mental state”. A practical method for grading
669 the cognitive state of patients for the clinician. *J. Psychiatr. Res.* 12, 189–198.
670 [https://doi.org/10.1016/0022-3956\(75\)90026-6](https://doi.org/10.1016/0022-3956(75)90026-6)

671 Friston, K.J., Ashburner, J., Kiebel, S., Nichols, T., Penny, W.D., 2007. Statistical parametric mapping :
672 the analysis of functional brain images. Elsevier Academic Press.

673 Friston, K.J., Harrison, L., Penny, W., 2003. Dynamic causal modelling. *Neuroimage* 19, 1273–1302.
674 [https://doi.org/10.1016/S1053-8119\(03\)00202-7](https://doi.org/10.1016/S1053-8119(03)00202-7)

675 Fuhrmann, D., Nesbitt, D., Shafto, M.A., Cam-CAN, Kievit, R.A., 2017. Cardiovascular Problems Predict
676 Poorer White Matter Health in the CamCAN Adult Lifespan Cohort.

677 Fukunaga, M., Li, T.-Q., van Gelderen, P., de Zwart, J.A., Shmueli, K., Yao, B., Lee, J., Maric, D., Aronova,
678 M.A., Zhang, G., Leapman, R.D., Schenck, J.F., Merkle, H., Duyn, J.H., 2010. Layer-specific variation
679 of iron content in cerebral cortex as a source of MRI contrast. *Proc. Natl. Acad. Sci. U. S. A.* 107,
680 3834–9. <https://doi.org/10.1073/pnas.0911177107>

681 Garrett, D.D., Lindenberger, U., Hoge, R.D., Gauthier, C.J., 2017. Age differences in brain signal
682 variability are robust to multiple vascular controls. *Sci. Rep.* 7, 10149.
683 <https://doi.org/10.1038/s41598-017-09752-7>

684 Ge, Q., Peng, W., Zhang, J., Weng, X., Zhang, Y., Liu, T., Zang, Y.-F., Wang, Z., 2017. Short-term apparent
685 brain tissue changes are contributed by cerebral blood flow alterations. *PLoS One* 12, e0182182.
686 <https://doi.org/10.1371/journal.pone.0182182>

687 Geerligs, L., Tsvetanov, K.A., 2016. The use of resting state data in an integrative approach to studying
688 neurocognitive ageing – Commentary on Campbell and Schacter (2016). *Lang. Cogn. Neurosci.* 32.
689 <https://doi.org/http://dx.doi.org/10.1080/23273798.2016.1251600>

690 Geerligs, L., Tsvetanov, K.A., Cam-Can, Henson, R.N., 2017. Challenges in measuring individual
691 differences in functional connectivity using fMRI: The case of healthy aging. *Hum. Brain Mapp.*
692 <https://doi.org/10.1002/hbm.23653>

693 Geyer, S., Weiss, M., Reimann, K., Lohmann, G., Turner, R., 2011. Microstructural Parcellation of the
694 Human Cerebral Cortex - From Brodmann's Post-Mortem Map to in vivo Mapping with High-Field
695 Magnetic Resonance Imaging. *Front. Hum. Neurosci.* 5, 19.
696 <https://doi.org/10.3389/fnhum.2011.00019>

697 Girouard, H., Iadecola, C., 2006. Neurovascular coupling in the normal brain and in hypertension, stroke,
698 and Alzheimer disease. *J. Appl. Physiol.* <https://doi.org/10.1152/japplphysiol.00966.2005>

699 Glasser, M.F., Van Essen, D.C., 2011. Mapping human cortical areas in vivo based on myelin content as
700 revealed by T1- and T2-weighted MRI. *J. Neurosci.* 31, 11597–616.
701 <https://doi.org/10.1523/JNEUROSCI.2180-11.2011>

702 Glover, G.H., Shmueli, K., van Gelderen, P., de Zwart, J. a, Horovitz, S.G., Fukunaga, M., Jansma, J.M.,
703 Duyn, J.H., 2007. Low-frequency fluctuations in the cardiac rate as a source of variance in the
704 resting-state fMRI BOLD signal. *Neuroimage* 38, 306–20.
705 <https://doi.org/10.1016/j.neuroimage.2007.07.037>

706 Goldberger, A.L., Amaral, L.A.N., Glass, L., Hausdorff, J.M., Ivanov, P.C., Mark, R.G., Mietus, J.E., Moody,
707 G.B., Peng, C.-K., Stanley, H.E., 2000. PhysioBank, PhysioToolkit, and PhysioNet. *Circulation* 101.
708 <https://doi.org/10.1161/01.CIR.101.23.e215>

709 Golestani, A.M., Chang, C., Kwint, J.B., Khatamian, Y.B., Jean Chen, J., 2015. Mapping the end-tidal CO2
710 response function in the resting-state BOLD fMRI signal: Spatial specificity, test–retest reliability
711 and effect of fMRI sampling rate. *Neuroimage* 104, 266–277.
712 <https://doi.org/10.1016/j.neuroimage.2014.10.031>

713 Golestani, A.M., Wei, L.L., Chen, J.J., 2016. Quantitative mapping of cerebrovascular reactivity using
714 resting-state BOLD fMRI: Validation in healthy adults. *Neuroimage* 138, 147–163.
715 <https://doi.org/10.1016/j.neuroimage.2016.05.025>

716 Goodman, E., Dolan, L.M., Morrison, J.A., Daniels, S.R., 2005. Factor Analysis of Clustered Cardiovascular
717 Risks in Adolescence. *Circulation* 111, 1970–1977.
718 <https://doi.org/10.1161/01.CIR.0000161957.34198.2B>

719 Grady, C.L., Garrett, D.D., 2013. Understanding variability in the BOLD signal and why it matters for
720 aging. *Brain Imaging Behav.* <https://doi.org/10.1007/s11682-013-9253-0>

721 Green, E., Bennett, H., Brayne, C., Tyler, L.K., Bullmore, E.T., Calder, A.C., Cusack, R., Dalgleish, T.,
722 Duncan, J., Henson, R.N., Marslen-Wilson, W.D., Rowe, J.B., Shafto, M.A., Campbell, K., Cheung,
723 T., Davis, S., Geerligs, L., Kievit, R., McCarrey, A., Mustafa, A., Price, D., Samu, D., Taylor, J.R.,
724 Treder, M., Tsvetanov, K., Van Belle, J., Williams, N., Bates, L., Emery, T., Erzinçlioglu, S., Gadie, A.,
725 Gerbase, S., Georgieva, S., Hanley, C., Parkin, B., Troy, D., Auer, T., Correia, M., Gao, L., Henriques,
726 R., Allen, J., Amery, G., Amunts, L., Barcroft, A., Castle, A., Dias, C., Dowrick, J., Fair, M., Fisher, H.,
727 Goulding, A., Grewal, A., Hale, G., Hilton, A., Johnson, F., Johnston, P., Kavanagh-Williamson, T.,
728 Kwasniewska, M., McMin, A., Norman, K., Penrose, J., Roby, F., Rowland, D., Sargeant, J., Squire,
729 M., Stevens, B., Stoddart, A., Stone, C., Thompson, T., Yazlik, O., Barnes, D., Dixon, M., Hillman, J.,
730 Mitchell, J., Willis, L., Matthews, F.E., 2018. Exploring patterns of response across the lifespan: The
731 Cambridge Centre for Ageing and Neuroscience (Cam-CAN) study. *BMC Public Health* 18.
732 <https://doi.org/10.1186/s12889-018-5663-7>

733 Gu, T., Fu, C., Shen, Z., Guo, H., Zou, M., Chen, M., Rockwood, K., Song, X., 2019. Age-Related Whole-
734 Brain Structural Changes in Relation to Cardiovascular Risks Across the Adult Age Spectrum. *Front.*
735 *Aging Neurosci.* 11, 85. <https://doi.org/10.3389/fnagi.2019.00085>

736 Hall, E.L., Driver, I.D., Croal, P.L., Francis, S.T., Gowland, P. a, Morris, P.G., Brookes, M.J., 2011. The effect
737 of hypercapnia on resting and stimulus induced MEG signals. *Neuroimage* 58, 1034–43.
738 <https://doi.org/10.1016/j.neuroimage.2011.06.073>

739 Hallquist, M.N., Hwang, K., Luna, B., 2013. The nuisance of nuisance regression: spectral
740 misspecification in a common approach to resting-state fMRI preprocessing reintroduces noise
741 and obscures functional connectivity. *Neuroimage* 82, 208–25.
742 <https://doi.org/10.1016/j.neuroimage.2013.05.116>

743 Handwerker, D. a, Gazzaley, A., Inglis, B. a, D’Esposito, M., 2007. Reducing vascular variability of fMRI
744 data across aging populations using a breathholding task. *Hum. Brain Mapp.* 28, 846–59.
745 <https://doi.org/10.1002/hbm.20307>

746 Hoge, R.D., Atkinson, J., Gill, B., Crelier, G.R., Marrett, S., Pike, G.B., 1999a. Investigation of BOLD signal
747 dependence on cerebral blood flow and oxygen consumption: The deoxyhemoglobin dilution
748 model. *Magn. Reson. Med.* 42, 849–863. [https://doi.org/10.1002/\(SICI\)1522-2594\(199911\)42:5<849::AID-MRM4>3.0.CO;2-Z](https://doi.org/10.1002/(SICI)1522-2594(199911)42:5<849::AID-MRM4>3.0.CO;2-Z)

750 Hoge, R.D., Atkinson, J., Gill, B., Crelier, G.R., Marrett, S., Pike, G.B., 1999b. Linear coupling between
751 cerebral blood flow and oxygen consumption in activated human cortex. *Proc. Natl. Acad. Sci. U.*
752 *S. A.* 96, 9403–9408. <https://doi.org/10.1073/pnas.96.16.9403>

753 Hui, M., Li, J., Wen, X., Yao, L., Long, Z., 2011. An empirical comparison of information-theoretic criteria
754 in estimating the number of independent components of fMRI data. *PLoS One* 6, e29274.
755 <https://doi.org/10.1371/journal.pone.0029274>

756 Jafarian, A., Litvak, V., Cagnan, H., Friston, K.J., Zeidman, P., 2020. Comparing dynamic causal models of
757 neurovascular coupling with fMRI and EEG/MEG. *Neuroimage* 216, 116734.
758 <https://doi.org/10.1016/j.neuroimage.2020.116734>

759 Jahanian, H., Christen, T., Moseley, M.E., Pajewski, N.M., Wright, C.B., Tamura, M.K., Zaharchuk, G.,
760 Group, for the S.S.R., 2017. Measuring vascular reactivity with resting-state blood oxygenation

level-dependent (BOLD) signal fluctuations: A potential alternative to the breath-holding challenge? *J. Cereb. Blood Flow Metab.* 37, 2526–2538. <https://doi.org/10.1177/0271678X16670921>

Jahanian, H., Ni, W.W., Christen, T., Moseley, M.E., Kurella Tamura, M., Zaharchuk, G., 2014. Spontaneous BOLD signal fluctuations in young healthy subjects and elderly patients with chronic kidney disease. *PLoS One* 9, e92539. <https://doi.org/10.1371/journal.pone.0092539>

Jenkinson, M., Bannister, P., Brady, M., Smith, S., 2002. Improved optimization for the robust and accurate linear registration and motion correction of brain images. *Neuroimage* 17, 825–41.

Kalcher, K., Boubela, R.N., Huf, W., Biswal, B.B., Baldinger, P., Sailer, U., Filzmoser, P., Kasper, S., Lamm, C., Lanzenberger, R., Moser, E., Windischberger, C., 2013. NeuroImage RESCALE : Voxel-specific task-fMRI scaling using resting state fluctuation amplitude. *Neuroimage* 70, 80–88. <https://doi.org/10.1016/j.neuroimage.2012.12.019>

Kannurpatti, S.S., Biswal, B.B., 2008. Detection and scaling of task-induced fMRI-BOLD response using resting state fluctuations. *Neuroimage* 40, 1567–74. <https://doi.org/10.1016/j.neuroimage.2007.09.040>

Kannurpatti, S.S., Motes, M. a, Rypma, B., Biswal, B.B., 2011. Increasing measurement accuracy of age-related BOLD signal change: minimizing vascular contributions by resting-state-fluctuation-of-amplitude scaling. *Hum. Brain Mapp.* 32, 1125–40. <https://doi.org/10.1002/hbm.21097>

Kazan, S.M., Mohammadi, S., Callaghan, M.F., Flandin, G., Huber, L., Leech, R., Kennerley, A., Windischberger, C., Weiskopf, N., 2016. Vascular autoresizing of fMRI (VasA fMRI) improves sensitivity of population studies: A pilot study. *Neuroimage* 124, 794–805. <https://doi.org/10.1016/j.neuroimage.2015.09.033>

Khader, Y.S., Batieha, A., Jaddou, H., Batieha, Z., El-Khateeb, M., Ajlouni, K., 2011. Factor Analysis of Cardiometabolic Risk Factors Clustering in Children and Adolescents. *Metab. Syndr. Relat. Disord.* 9, 151–156. <https://doi.org/10.1089/met.2010.0097>

Krainik, A., Hund-Georgiadis, M., Zysset, S., von Cramon, D.Y., 2005. Regional Impairment of Cerebrovascular Reactivity and BOLD Signal in Adults After Stroke. *Stroke* 36, 1146–1152. <https://doi.org/10.1161/01.STR.0000166178.40973.a7>

Kumral, D., Şansal, F., Cesnaite, E., Mahjoory, K., Al, E., Gaebler, M., Nikulin, V. V., Villringer, A., 2019. BOLD and EEG Signal Variability at Rest Differently Relate to Aging in the Human Brain. *bioRxiv* 646273. <https://doi.org/10.1101/646273>

Lee, H.-Y., Oh, B.-H., 2010. Aging and arterial stiffness. *Circ. J.* 74, 2257–62.

Li, Y.-O., Adali, T., Calhoun, V.D., 2007. Estimating the number of independent components for functional magnetic resonance imaging data. *Hum. Brain Mapp.* 28, 1251–66. <https://doi.org/10.1002/hbm.20359>

Liau, J., Liu, T.T., 2009. Inter-subject variability in hypercapnic normalization of the BOLD fMRI response. *Neuroimage* 45, 420–30. <https://doi.org/10.1016/j.neuroimage.2008.11.032>

Lindquist, M.A., Geuter, S., Wager, T.D., Caffo, B.S., 2019. Modular preprocessing pipelines can reintroduce artifacts into fMRI data. *Hum. Brain Mapp.* 40, 2358–2376. <https://doi.org/10.1002/hbm.24528>

Lipp, I., Murphy, K., Caseras, X., Wise, R.G., 2015. Agreement and repeatability of vascular reactivity estimates based on a breath-hold task and a resting state scan. *Neuroimage* 113, 387–396. <https://doi.org/10.1016/j.neuroimage.2015.03.004>

804 Liu, K., Yao, S., Chen, K., Zhang, J., Yao, L., Li, K., Jin, Z., Guo, X., 2017. Structural Brain Network Changes
805 across the Adult Lifespan. *Front. Aging Neurosci.* 9, 275.
806 <https://doi.org/10.3389/fnagi.2017.00275>

807 Liu, P., De Vis, J.B., Lu, H., 2019. Cerebrovascular reactivity (CVR) MRI with CO2 challenge: A technical
808 review. *Neuroimage* 187, 104–115. <https://doi.org/10.1016/J.NEUROIMAGE.2018.03.047>

809 Liu, P., Hebrank, A.C., Rodrigue, K.M., Kennedy, K.M., Park, D.C., Lu, H., 2012. A comparison of
810 physiologic modulators of fMRI signals. *Hum. Brain Mapp.* 00, 2078–88.
811 <https://doi.org/10.1002/hbm.22053>

812 Liu, P., Hebrank, A.C., Rodrigue, K.M., Kennedy, K.M., Section, J., Park, D.C., Lu, H., 2013. Age-related
813 differences in memory-encoding fMRI responses after accounting for decline in vascular
814 reactivity. *Neuroimage* 78, 415–25. <https://doi.org/10.1016/j.neuroimage.2013.04.053>

815 Liu, P., Li, Y., Pinho, M., Park, D.C., Welch, B.G., Lu, H., 2017. Cerebrovascular reactivity mapping without
816 gas challenges. *Neuroimage* 146, 320–326. <https://doi.org/10.1016/j.neuroimage.2016.11.054>

817 Logothetis, N.K., 2008. What we can do and what we cannot do with fMRI. *Nature* 453, 869–878.
818 <https://doi.org/10.1038/nature06976>

819 Lu, H., Yezhuvath, U.S., Xiao, G., 2010. Improving fMRI sensitivity by normalization of basal physiologic
820 state. *Hum. Brain Mapp.* 31, 80–7. <https://doi.org/10.1002/hbm.20846>

821 Magon, S., Basso, G., Farace, P., Ricciardi, G.K., Beltramello, A., Sbarbati, A., 2009. Reproducibility of
822 BOLD signal change induced by breath holding. *Neuroimage* 45, 702–712.
823 <https://doi.org/10.1016/J.NEUROIMAGE.2008.12.059>

824 Makedonov, I., Black, S.E., Macintosh, B.J., 2013. BOLD fMRI in the white matter as a marker of aging
825 and small vessel disease. *PLoS One* 8, e67652. <https://doi.org/10.1371/journal.pone.0067652>

826 Malik, M., Bigger, J.T., Camm, A.J., Kleiger, R.E., Malliani, A., Moss, A.J., Schwartz, P.J., 1996. Heart rate
827 variability: Standards of measurement, physiological interpretation, and clinical use. *Eur. Heart J.*
828 17, 354–381. <https://doi.org/10.1093/oxfordjournals.eurheartj.a014868>

829 Mayer-Davis, E.J., Ma, B., Lawson, A., D’Agostino, R.B., Liese, A.D., Bell, R.A., Dabelea, D., Dolan, L.,
830 Pettitt, D.J., Rodriguez, B.L., Williams, D., SEARCH for Diabetes in Youth Study Group, D., 2009.
831 Cardiovascular disease risk factors in youth with type 1 and type 2 diabetes: implications of a
832 factor analysis of clustering. *Metab. Syndr. Relat. Disord.* 7, 89–95.
833 <https://doi.org/10.1089/met.2008.0046>

834 Mayhew, S.D., Li, S., Storrar, J.K., Tsvetanov, K.A., Kourtzi, Z., 2010. Learning shapes the representation
835 of visual categories in the aging human brain. *J. Cogn. Neurosci.* 22.
836 <https://doi.org/10.1162/jocn.2010.21415>

837 Millar, P.R., Petersen, S.E., Ances, B.M., Gordon, B.A., Benzinger, T.L.S., Morris, J.C., Balota, D.A., 2020.
838 Evaluating the Sensitivity of Resting-State BOLD Variability to Age and Cognition after Controlling
839 for Motion and Cardiovascular Influences: A Network-Based Approach. *Cereb. Cortex* 00, 1–16.
840 <https://doi.org/10.1093/cercor/bhaa138>

841 Mohajer, B., Abbasi, N., Mohammadi, E., Khazaie, H., Osorio, R.S., Rosenzweig, I., Eickhoff, C.R., Zarei,
842 M., Tahmasian, M., Eickhoff, S.B., 2020. Gray matter volume and estimated brain age gap are not
843 linked with <sc>sleep-disordered</sc> breathing. *Hum. Brain Mapp.* hbm.24995.
844 <https://doi.org/10.1002/hbm.24995>

845 Mueller, S., Wang, D., Fox, M.D., Yeo, B.T.T., Sepulcre, J., Sabuncu, M.R., Shafee, R., Lu, J., Liu, H., 2013.
846 Individual Variability in Functional Connectivity Architecture of the Human Brain. *Neuron* 77, 586–

847 595. <https://doi.org/10.1016/j.neuron.2012.12.028>

848 Mutsaerts, H.J., Petr, J., Václavů, L., van Dalen, J.W., Robertson, A.D., Caan, M.W., Masellis, M.,
849 Nederveen, A.J., Richard, E., MacIntosh, B.J., 2017. The spatial coefficient of variation in arterial
850 spin labeling cerebral blood flow images. *J. Cereb. Blood Flow Metab.* 37, 3184–3192.
851 <https://doi.org/10.1177/0271678X16683690>

852 Mutsaerts, H.J.M.M., Petr, J., Thomas, D.L., De Vita, E., Cash, D.M., van Osch, M.J.P., Golay, X., Groot,
853 P.F.C., Ourselin, S., van Swieten, J., Laforce, R., Tagliavini, F., Borroni, B., Galimberti, D., Rowe, J.B.,
854 Graff, C., Pizzini, F.B., Finger, E., Sorbi, S., Castelo Branco, M., Rohrer, J.D., Masellis, M., MacIntosh,
855 B.J., GENFI investigators, 2018. Comparison of arterial spin labeling registration strategies in the
856 multi-center GENetic frontotemporal dementia initiative (GENFI). *J. Magn. Reson. Imaging* 47,
857 131–140. <https://doi.org/10.1002/jmri.25751>

858 O'Rourke, M.F., Hashimoto, J., 2007. Mechanical factors in arterial aging: a clinical perspective. *J. Am.*
859 *Coll. Cardiol.* 50, 1–13. <https://doi.org/10.1016/j.jacc.2006.12.050>

860 Oldfield, R.C., 1971. The assessment and analysis of handedness: the Edinburgh inventory.
861 *Neuropsychologia* 9, 97–113.

862 Passamonti, L., Tsvetanov, K.A., Jones, P.S., Bevan-Jones, W.R., Arnold, R., Borchert, R.J., Mak, E., Su, L.,
863 O'Brien, J.T., Rowe, J.B., Passamonti, Luca, 2019. Neuroinflammation and functional connectivity
864 in Alzheimer's disease: interactive influences on cognitive performance. *bioRxiv Prepr.*
865 <https://doi.org/10.1101/532291>

866 Patel, A.X., Kundu, P., Rubinov, M., Simon Jones, P., Vértes, P.E., Ersche, K.D., Suckling, J., Bullmore, E.T.,
867 2014. A wavelet method for modeling and despiking motion artifacts from resting-state fMRI time
868 series. *Neuroimage.* <https://doi.org/10.1016/j.neuroimage.2014.03.012>

869 Peelle, J.E., Cusack, R., Henson, R.N. a, 2012. Adjusting for global effects in voxel-based morphometry:
870 Gray matter decline in normal aging. *Neuroimage* 60, 1503–1516.
871 <https://doi.org/10.1016/j.neuroimage.2011.12.086>

872 Restom, K., Bangen, K.J., Bondi, M.W., Perthen, J.E., Liu, T.T., 2007. Cerebral blood flow and BOLD
873 responses to a memory encoding task: a comparison between healthy young and elderly adults.
874 *Neuroimage* 37, 430–9. <https://doi.org/10.1016/j.neuroimage.2007.05.024>

875 Riecker, A., Grodd, W., Klose, U., Schulz, J.B., Gröschel, K., Erb, M., Ackermann, H., Kastrup, A., 2003.
876 Relation between regional functional MRI activation and vascular reactivity to carbon dioxide
877 during normal aging. *J. Cereb. Blood Flow Metab.* 23, 565–73.
878 <https://doi.org/10.1097/01.WCB.0000056063.25434.04>

879 Rissanen, J., 1978. Modeling by shortest data description. *Automatica* 14, 465–471.
880 [https://doi.org/10.1016/0005-1098\(78\)90005-5](https://doi.org/10.1016/0005-1098(78)90005-5)

881 Robertson, A.D., Matta, G., Basile, V.S., Black, S.E., Macgowan, C.K., Detre, J.A., MacIntosh, B.J., 2017.
882 Temporal and spatial variances in arterial spin-labeling are inversely related to large-artery blood
883 velocity. *Am. J. Neuroradiol.* 38, 1555–1561. <https://doi.org/10.3174/ajnr.A5257>

884 Robertson, A.D., Tessmer, C.F., Hughson, R.L., 2010. Association between arterial stiffness and
885 cerebrovascular resistance in the elderly. *J. Hum. Hypertens.* 24, 190–196.
886 <https://doi.org/10.1038/jhh.2009.56>

887 Sami, S., Miall, R.C., 2013. Graph network analysis of immediate motor-learning induced changes in
888 resting state BOLD. *Front. Hum. Neurosci.* 7, 166. <https://doi.org/10.3389/fnhum.2013.00166>

889 Sami, S., Robertson, E.M., Miall, R.C., 2014. The time course of task-specific memory consolidation

890 effects in resting state networks. *J. Neurosci.* 34, 3982–92.
891 <https://doi.org/10.1523/JNEUROSCI.4341-13.2014>

892 Samu, D., Campbell, K.L., Tsvetanov, K.A., Shafto, M.A., Consortium, C.-C., Brayne, C., Bullmore, E.T.,
893 Calder, A.C., Cusack, R., Dalgleish, T., Duncan, J., Henson, R.N., Matthews, F.E., Marslen-Wilson,
894 W.D., Rowe, J.B., Cheung, T., Davis, S., Geerligs, L., Kievit, R., McCarrey, A., Mustafa, A., Price, D.,
895 Taylor, J.R., Treder, M., Belle, J. van, Williams, N., Bates, L., Emery, T., Erzinçlioglu, S., Gadie, A.,
896 Gerbase, S., Georgieva, S., Hanley, C., Parkin, B., Troy, D., Auer, T., Correia, M., Gao, L., Green, E.,
897 Henriques, R., Allen, J., Amery, G., Amunts, L., Barcroft, A., Castle, A., Dias, C., Dowrick, J., Fair, M.,
898 Fisher, H., Goulding, A., Grewal, A., Hale, G., Hilton, A., Johnson, F., Johnston, P., Kavanagh-
899 Williamson, T., Kwasniewska, M., McMinn, A., Norman, K., Penrose, J., Roby, F., Rowland, D.,
900 Sargeant, J., Squire, M., Stevens, B., Stoddart, A., Stone, C., Thompson, T., Yazlik, O., Barnes, D.,
901 Dixon, M., Hillman, J., Mitchell, J., Villis, L., Tyler, L.K., 2017. Preserved cognitive functions with
902 age are determined by domain-dependent shifts in network responsivity. *Nat. Commun.* 8,
903 ncomms14743. <https://doi.org/10.1038/ncomms14743>

904 Satterthwaite, T.D., Elliott, M. a, Gerraty, R.T., Ruparel, K., Loughhead, J., Calkins, M.E., Eickhoff, S.B.,
905 Hakonarson, H., Gur, R.C.R.E., Gur, R.C.R.E., Wolf, D.H., 2013. An improved framework for
906 confound regression and filtering for control of motion artifact in the preprocessing of resting-
907 state functional connectivity data. *Neuroimage* 64, 240–56.
908 <https://doi.org/10.1016/j.neuroimage.2012.08.052>

909 Shafto, M.A., Tyler, L.K., Dixon, M., Taylor, J.R., Rowe, J.B., Cusack, R., Calder, A.J., Marslen-Wilson, W.D.,
910 Duncan, J., Dalgleish, T., Henson, R.N., Brayne, C., Bullmore, E., Campbell, K., Cheung, T., Davis, S.,
911 Geerligs, L., Kievit, R., McCarrey, A., Price, D., Samu, D., Treder, M., Tsvetanov, K., Williams, N.,
912 Bates, L., Emery, T., Erzinçlioglu, S., Gadie, A., Gerbase, S., Georgieva, S., Hanley, C., Parkin, B.,
913 Troy, D., Allen, J., Amery, G., Amunts, L., Barcroft, A., Castle, A., Dias, C., Dowrick, J., Fair, M., Fisher,
914 H., Goulding, A., Grewal, A., Hale, G., Hilton, A., Johnson, F., Johnston, P., Kavanagh-Williamson,
915 T., Kwasniewska, M., McMinn, A., Norman, K., Penrose, J., Roby, F., Rowland, D., Sargeant, J.,
916 Squire, M., Stevens, B., Stoddart, A., Stone, C., Thompson, T., Yazlik, O., Barnes, D., Hillman, J.,
917 Mitchell, J., Villis, L., Matthews, F.E., 2014. The Cambridge Centre for Ageing and Neuroscience
918 (Cam-CAN) study protocol: A cross-sectional, lifespan, multidisciplinary examination of healthy
919 cognitive ageing. *BMC Neurol.* 14. <https://doi.org/10.1186/s12883-014-0204-1>

920 Skinner, H.A., 1982. The drug abuse screening test. *Addict. Behav.* 7, 363–71.

921 Snellen, H., 1862. *Probabuchstaben zur bestimmung der sehscharfe*. Van de Weijer, Utrecht.

922 Srinivasa, R.N., Rossetti, H.C., Gupta, M.K., Rosenberg, R.N., Weiner, M.F., Peshock, R.M., McColl, R.W.,
923 Hynan, L.S., Lucarelli, R.T., King, K.S., 2016. Cardiovascular Risk Factors Associated with Smaller
924 Brain Volumes in Regions Identified as Early Predictors of Cognitive Decline. *Radiology* 278, 198–
925 204. <https://doi.org/10.1148/radiol.2015142488>

926 Sui, J., Adali, T., Yu, Q., Chen, J., Calhoun, V.D., 2012. A review of multivariate methods for multimodal
927 fusion of brain imaging data. *J. Neurosci. Methods* 204, 68–81.
928 <https://doi.org/10.1016/j.jneumeth.2011.10.031>

929 Tardif, C.L., Steele, C.J., Lampe, L., Bazin, P.-L., Ragert, P., Villringer, A., Gauthier, C.J., 2017. Investigation
930 of the confounding effects of vasculature and metabolism on computational anatomy studies.
931 *Neuroimage* 149, 233–243. <https://doi.org/10.1016/J.NEUROIMAGE.2017.01.025>

932 Tarumi, T., Ayaz Khan, M., Liu, J., Tseng, B.M., Parker, R., Riley, J., Tinajero, C., Zhang, R., 2014. Cerebral
933 hemodynamics in normal aging: central artery stiffness, wave reflection, and pressure pulsatility.
934 *J. Cereb. Blood Flow Metab.* 34, 971–8. <https://doi.org/10.1038/jcbfm.2014.44>

935 Tarumi, T., Zhang, R., 2018. Cerebral blood flow in normal aging adults: cardiovascular determinants,

clinical implications, and aerobic fitness. *J. Neurochem.* 144, 595–608.
<https://doi.org/10.1111/jnc.14234>

Taylor, J.R., Williams, N., Cusack, R., Auer, T., Shafto, M.A., Dixon, M., Tyler, L.K., Cam-Can, Henson, R.N.,
 2015. The Cambridge Centre for Ageing and Neuroscience (Cam-CAN) data repository: Structural
 and functional MRI, MEG, and cognitive data from a cross-sectional adult lifespan sample.
Neuroimage. <https://doi.org/10.1016/j.neuroimage.2015.09.018>

Theyers, A.E., Goldstein, B.I., Metcalfe, A.W., Robertson, A.D., MacIntosh, B.J., 2018. Cerebrovascular
 blood oxygenation level dependent pulsatility at baseline and following acute exercise among
 healthy adolescents. *J. Cereb. Blood Flow Metab.* 0271678X1876677.
<https://doi.org/10.1177/0271678X18766771>

Thomason, M.E., Burrows, B.E., Gabrieli, J.D.E., Glover, G.H., 2005. Breath holding reveals differences
 in fMRI BOLD signal in children and adults. *Neuroimage* 25, 824–37.
<https://doi.org/10.1016/j.neuroimage.2004.12.026>

Thomason, M.E., Foland, L.C., Glover, G.H., 2007. Calibration of BOLD fMRI using breath holding reduces
 group variance during a cognitive task. *Hum. Brain Mapp.* 28, 59–68.
<https://doi.org/10.1002/hbm.20241>

Tsvetanov, K.A., Gazzina, S., Jones, S.P., Swieten, J. van, Borroni, B., Sanchez-Valle, R., Moreno, F.,
 Laforce, R., Graff, C., Synofzik, M., Galimberti, D., Masellis, M., Tartaglia, M.C., Finger, E.,
 Vandenberghe, R., Mendonça, A. de, Tagliavini, F., Santana, I., Ducharne, S., Butler, C., Gerhard,
 A., Danek, A., Levin, J., Otto, M., Frisoni, G., Ghidoni, R., Sorbi, S., Rohrer, J.D., Rowe, J.B., (GENFI),
 T.G.F.I., 2019. Brain functional network integrity sustains cognitive function despite atrophy in
 presymptomatic genetic frontotemporal dementia. *medRxiv* 19012203.
<https://doi.org/10.1101/19012203>

Tsvetanov, K.A., Henson, R.N.A., Rowe, J.B., 2020. Separating vascular and neuronal effects of age on
 fMRI BOLD signals. *Philos. Trans. R. Soc. B Biol. Sci.* <https://doi.org/10.1098/rstb.2019.0631>

Tsvetanov, K.A., Henson, R.N.A., Tyler, L.K., Davis, S.W., Shafto, M.A., Taylor, J.R., Williams, N., Rowe,
 J.B., 2015. The effect of ageing on fMRI: Correction for the confounding effects of vascular
 reactivity evaluated by joint fMRI and MEG in 335 adults. *Hum. Brain Mapp.* 36, 2248–2269.
<https://doi.org/10.1002/hbm.22768>

Tsvetanov, K.A., Henson, R.N.A., Tyler, L.K., Razi, A., Geerligs, L., Ham, T.E., Rowe, J.B., 2016. Extrinsic
 and intrinsic brain network connectivity maintains cognition across the lifespan despite
 accelerated decay of regional brain activation. *J. Neurosci.* 36, 3115–26.
<https://doi.org/10.1523/JNEUROSCI.2733-15.2016>

Tsvetanov, K.A., Ye, Z., Hughes, L., Samu, D., Treder, M.S., Wolpe, N., Tyler, L.K., Rowe, J.B., for
 Cambridge Centre for Ageing and Neuroscience, 2018. Activity and connectivity differences
 underlying inhibitory control across the adult lifespan. *J. Neurosci.* 38, 7887–7900.
<https://doi.org/10.1523/JNEUROSCI.2919-17.2018>

Varadhan, R., Chaves, P.H.M., Lipsitz, L.A., Stein, P.K., Tian, J., Windham, B.G., Berger, R.D., Fried, L.P.,
 2009. Frailty and impaired cardiac autonomic control: new insights from principal components
 aggregation of traditional heart rate variability indices. *J. Gerontol. A. Biol. Sci. Med. Sci.* 64, 682–
 7. <https://doi.org/10.1093/gerona/glp013>

Vest, A.N., Da Poian, G., Li, Q., Liu, C., Nemati, S., Shah, A.J., Clifford, G.D., 2018. An open source
 benchmarked toolbox for cardiovascular waveform and interval analysis. *Physiol. Meas.* 39,
 105004. <https://doi.org/10.1088/1361-6579/aae021>

- Viessmann, O., Möller, H.E., Jezzard, P., 2019. Dual regression physiological modeling of resting-state EPI power spectra: Effects of healthy aging. *Neuroimage* 187, 68–76. <https://doi.org/10.1016/J.NEUROIMAGE.2018.01.011>
- Viessmann, O., Möller, H.E., Jezzard, P., 2017. Cardiac cycle-induced EPI time series fluctuations in the brain: Their temporal shifts, inflow effects and T2* fluctuations. *Neuroimage* 162, 93–105. <https://doi.org/10.1016/J.NEUROIMAGE.2017.08.061>
- Wardlaw, J.M., Allerhand, M., Doubal, F.N., Valdes Hernandez, M., Morris, Z., Gow, A.J., Bastin, M., Starr, J.M., Dennis, M.S., Deary, I.J., 2014. Vascular risk factors, large-artery atheroma, and brain white matter hyperintensities. *Neurology* 82, 1331–8. <https://doi.org/10.1212/WNL.0000000000000312>
- Webb, A.J.S., Rothwell, P.M., 2014. Physiological Correlates of Beat-to-Beat, Ambulatory, and Day-to-Day Home Blood Pressure Variability After Transient Ischemic Attack or Minor Stroke. *Stroke* 45, 533–538. <https://doi.org/10.1161/STROKEAHA.113.003321>
- Webb, A.J.S., Simoni, M., Mazzucco, S., Kuker, W., Schulz, U., Rothwell, P.M., 2012. Increased Cerebral Arterial Pulsatility in Patients With Leukoaraiosis. *Stroke* 43, 2631–2636. <https://doi.org/10.1161/STROKEAHA.112.655837>
- West, K.L., Zuppichini, M.D., Turner, M.P., Sivakolundu, D.K., Zhao, Y., Abdelkarim, D., Spence, J.S., Rypma, B., 2019. BOLD hemodynamic response function changes significantly with healthy aging. *Neuroimage* 188, 198–207. <https://doi.org/10.1016/j.neuroimage.2018.12.012>
- Whittaker, J.R., Driver, I.D., Bright, M.G., Murphy, K., 2016. The absolute CBF response to activation is preserved during elevated perfusion: Implications for neurovascular coupling measures. *Neuroimage* 125, 198–207. <https://doi.org/10.1016/j.neuroimage.2015.10.023>
- Xu, J., Potenza, M.N., Calhoun, V.D., 2013. Spatial ICA reveals functional activity hidden from traditional fMRI GLM-based analyses. *Front. Neurosci.* 7, 1–4. <https://doi.org/10.3389/fnins.2013.00154>
- Xu, L., Groth, K.M., Pearlson, G., Schretlen, D.J., Calhoun, V.D., 2009. Source-based morphometry: the use of independent component analysis to identify gray matter differences with application to schizophrenia. *Hum. Brain Mapp.* 30, 711–24. <https://doi.org/10.1002/hbm.20540>
- Yezhuvath, U.S., Lewis-Amezcu, K., Varghese, R., Xiao, G., Lu, H., 2009. On the assessment of cerebrovascular reactivity using hypercapnia BOLD MRI. *NMR Biomed.* 22, 779–86. <https://doi.org/10.1002/nbm.1392>
- Zhang, N., Gordon, M.L., Ma, Y., Chi, B., Gomar, J.J., Peng, S., Kingsley, P.B., Eidelberg, D., Goldberg, T.E., 2018. The Age-Related Perfusion Pattern Measured With Arterial Spin Labeling MRI in Healthy Subjects. *Front. Aging Neurosci.* 10, 214. <https://doi.org/10.3389/fnagi.2018.00214>
- Zlokovic, B. V., 2011. Neurovascular pathways to neurodegeneration in Alzheimer’s disease and other disorders. *Nat. Rev. Neurosci.* 12, 723–38. <https://doi.org/10.1038/nrn3114>

7. Tables

Table 1. Participants' demographic information, grouped by decile in accordance with the original design of the Cam-CAN cohort (Green et al., 2018; Shafito et al., 2014)

	Decile							Statistical tests*	
	1	2	3	4	5	6	7	χ^2 or F-test	P-value
Age range [years]	18-27	28-37	38-47	48-57	58-67	68-77	78-90		
Gender, n (% per decile)								0.15	0.989
Men	7 (46.7)	19 (46.3)	19 (50)	19 (52.8)	19 (50)	17 (56.7)	14 (50)		
Women	8 (53.3)	22 (53.7)	19 (50)	17 (47.2)	19 (50)	13 (43.3)	14 (50)		
Handedness**								1.34	0.241
Mean / SD	91 / 12	85 / 42	86 / 27	93 / 11	79 / 48	97 / 5	91 / 30		
Range [Min/Max]	65 / 100	-65 / 100	-56 / 100	58 / 100	-78 / 100	86 / 100	-56 / 100		
Education, n (% per decile)								4.07	<.001
None	0 (0)	0 (0)	0 (0)	0 (0)	0 (0)	5 (16.7)	1 (3.6)		
GCSE/O-level	2 (13.3)	1 (2.4)	6 (15.8)	3 (8.3)	4 (10.5)	2 (6.7)	4 (14.3)		
A-level	2 (13.3)	2 (4.9)	3 (7.9)	12 (33.3)	9 (23.7)	9 (30)	8 (28.6)		
Degree	11 (73.3)	38 (92.7)	29 (76.3)	21 (58.3)	25 (65.8)	14 (46.7)	15 (53.6)		
Mini-Mental State Exam								3.17	0.006
Mean / SD	29.5 / 0.9	29.6 / 0.7	29.1 / 1.2	29.2 / 0.9	29.1 / 1	28.7 / 1.3	28.8 / 1.3		
Range [Min/Max]	27 / 30	27 / 30	26 / 30	26 / 30	27 / 30	26 / 30	25 / 30		

* Statistical test to indicate whether demographics vary between deciles

** Higher scores indicate greater right-hand preference

Table 2. Evaluation of the difference in distribution shape across voxels in the whole brain, as well as voxels within grey matter (GM), white matter (WM) and cerebrospinal fluid (CSF) areas. Tests showing no difference in the distributions at uncorrected p-value 0.05 are indicated by n.s.

Model	Whole Brain	GM	WM	CSF
1	<0.001	<0.001	0.009	<0.001
2	<0.001	<0.001	0.009	<0.001
3	0.015	n.s.	0.048	0.005
4	0.016	n.s.	0.039	0.007
5	<0.001	<0.001	0.004	<0.001

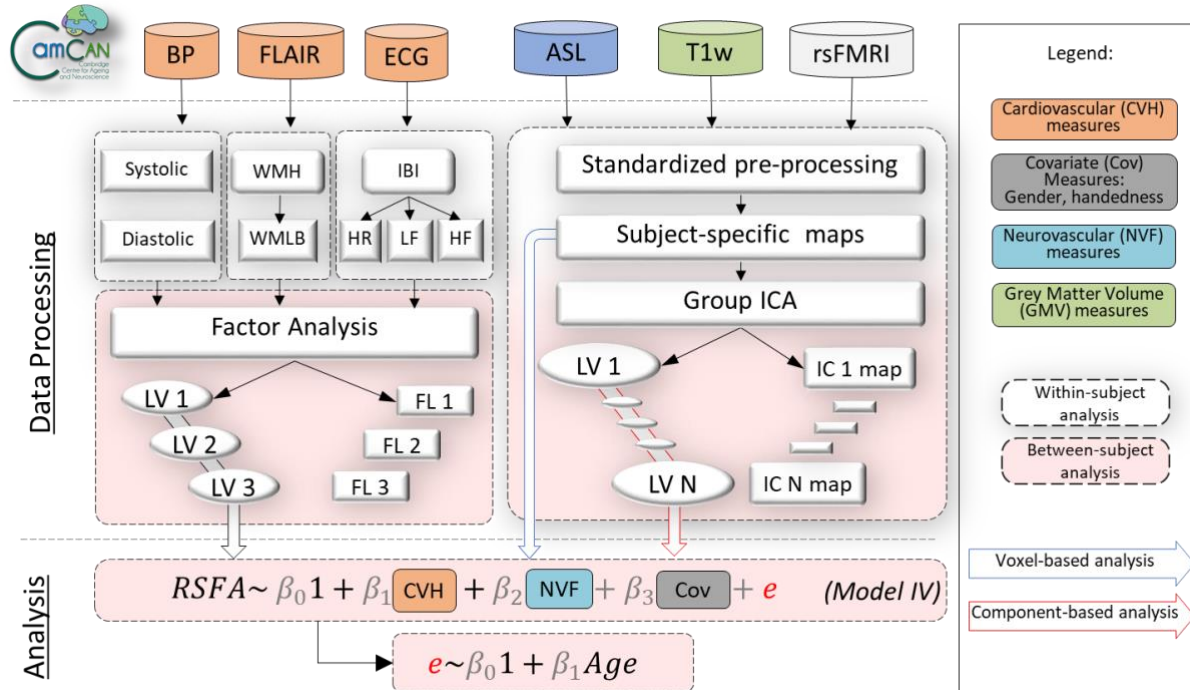


Figure 1. Visual representation of the analysis strategy in terms of data inclusion (above top dotted line), processing (below top dotted line) either at a within-subject level (white dotted-line rectangles) or between-subject level (peach-color dotted-line rectangles) and analysis (below second dotted line). Measures of cardiovascular health (CVH) included blood pressure (BP), heart rate variability (HRV) from electrocardiogram (ECG) recordings, white matter-matter hyperintensities (WMH) from fluid-attenuated inversion recovery (FLAIR) and BMI (not shown), all of which were submitted to factor analysis. Neurovascular function (NVF) estimates were based on cerebral blood flow from arterial spin labelling (ASL) acquisition. Grey matter volume (GMV) was estimated from a T1-weighted MRI acquisition. Resting state fluctuation amplitudes (RSFA) were estimated from resting-state fMRI BOLD acquisition. Regionally specific measures (RSFA, CBF and GMV) were submitted to multiple linear regression either on a voxel-level or on a component-level using outputs from group ICA. ICA – independent component analysis; LV – latent variable; LST – lesion-segmentation tool; PCA – principal component analysis; rsfMRI – resting state fMRI; TLV – total lesion volume; WMLB – white-matter lesion burden;

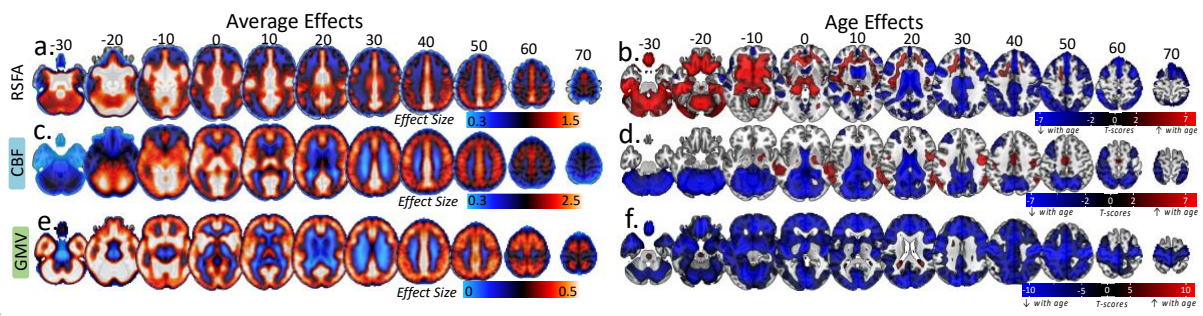
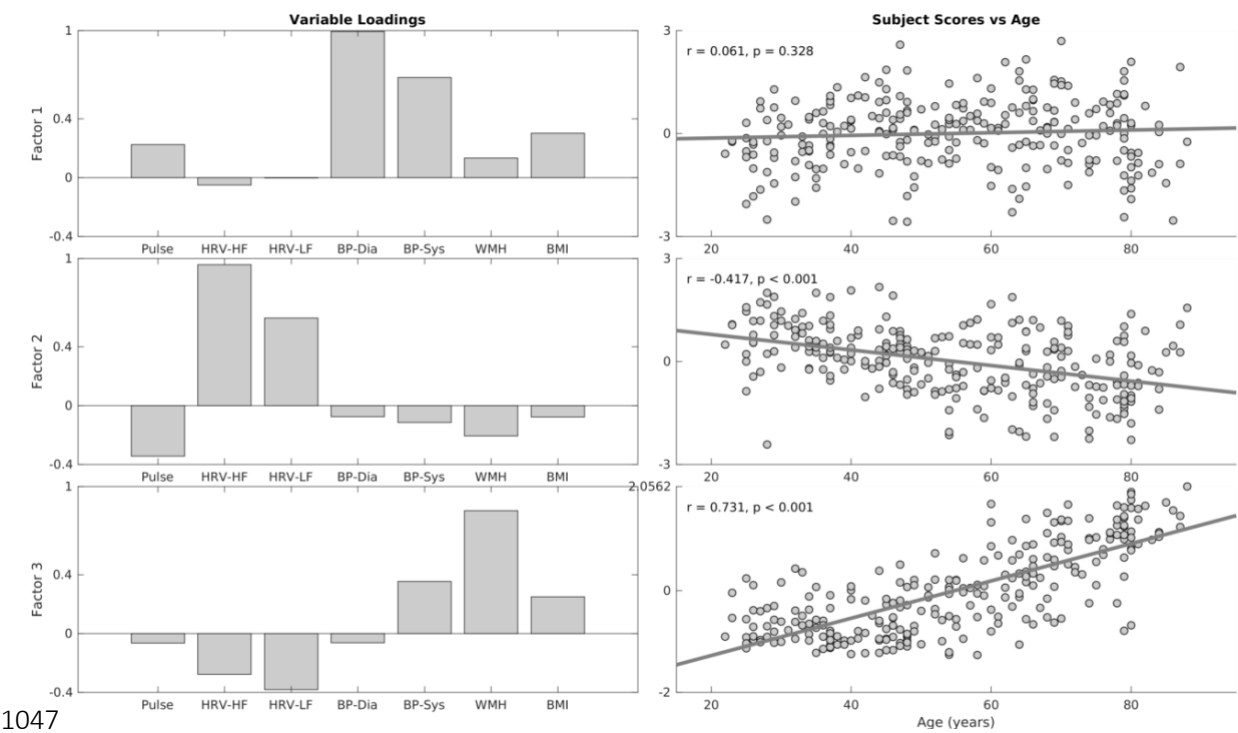


Figure 2. Average RSFA, CBF and Grey Matter Volume and the effects of age on each modality (SPM{beta} and SPM{t} maps respectively)

1046



1047

1048

1049

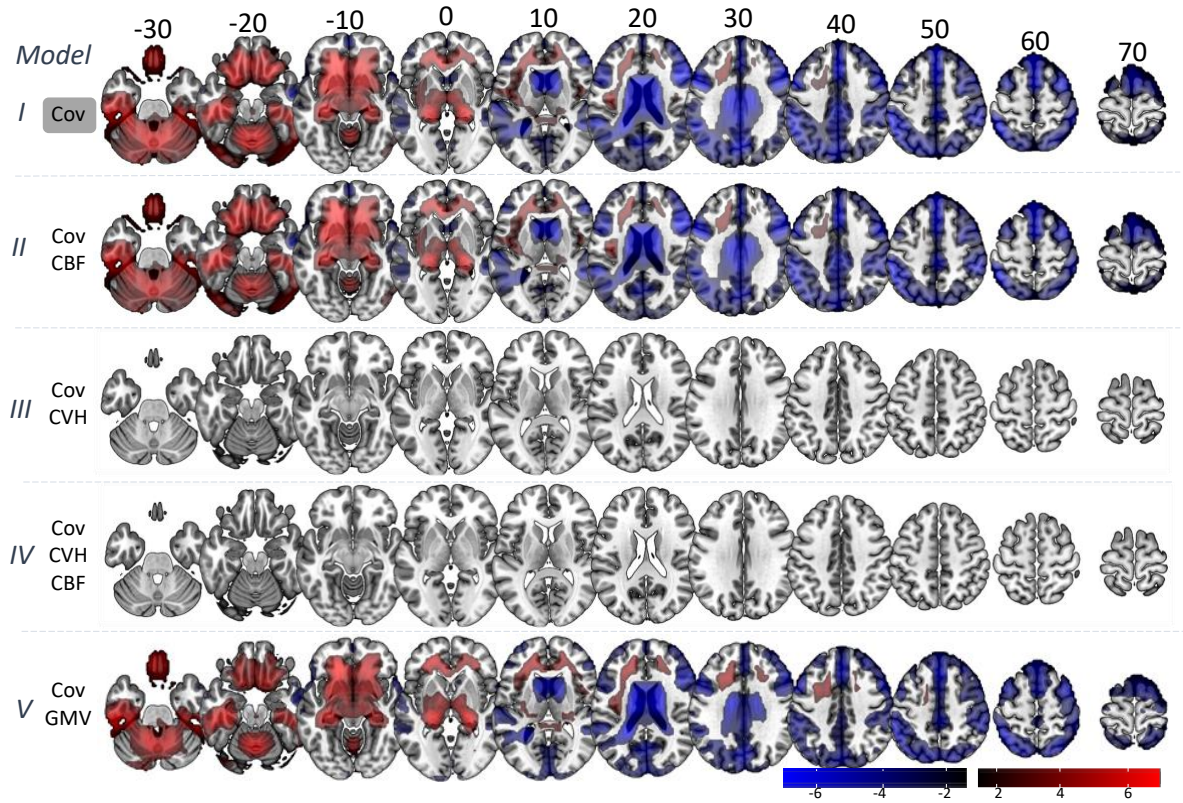
1050

1051

1052

Figure 3. Variable loadings (left column) and association between age and subjects scores for three factors resulting from factor analysis on cardiovascular risk variables. Pulse – mean heart rate, HRV-HF – high-frequency heart rate variability, HRV-LF – low-frequency high rate variability, BP-Dia – diastolic blood pressure, BP-Sys – systolic blood pressure, WMH – white matter hyperintensities, BMI – body-mass index

1053



1054

1055

1056

1057

1058

1059

Figure 4. Voxel-wise associations between age and RSFA residuals after controlling for: covariates only (Cov, Model I); Cov and cerebral blood flow (CBF, Model II); Cov and cardiovascular health (CVH, Model III); Cov, CBF and CVH (Model IV); and Cov and grey matter volume (GMV).

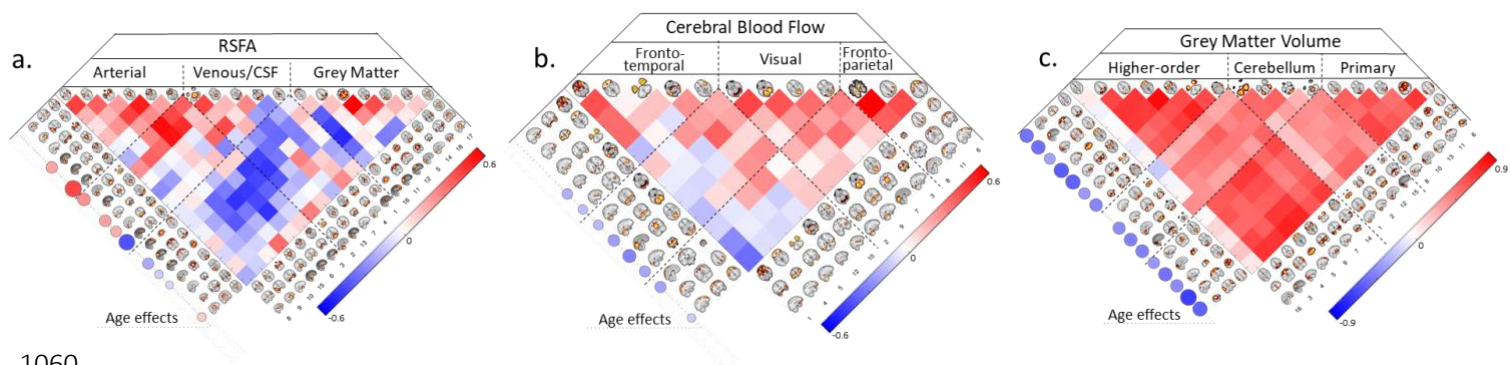


Figure 5 Independent component analysis spatial maps and correlation between subject loadings for RSFA (a), cerebral blood flow (b) and grey matter volume (c) datasets. The relationships between age and IC loadings are shown circles on the left hand-side of each correlation matrix, FDR-adjusted p -value of 0.05.

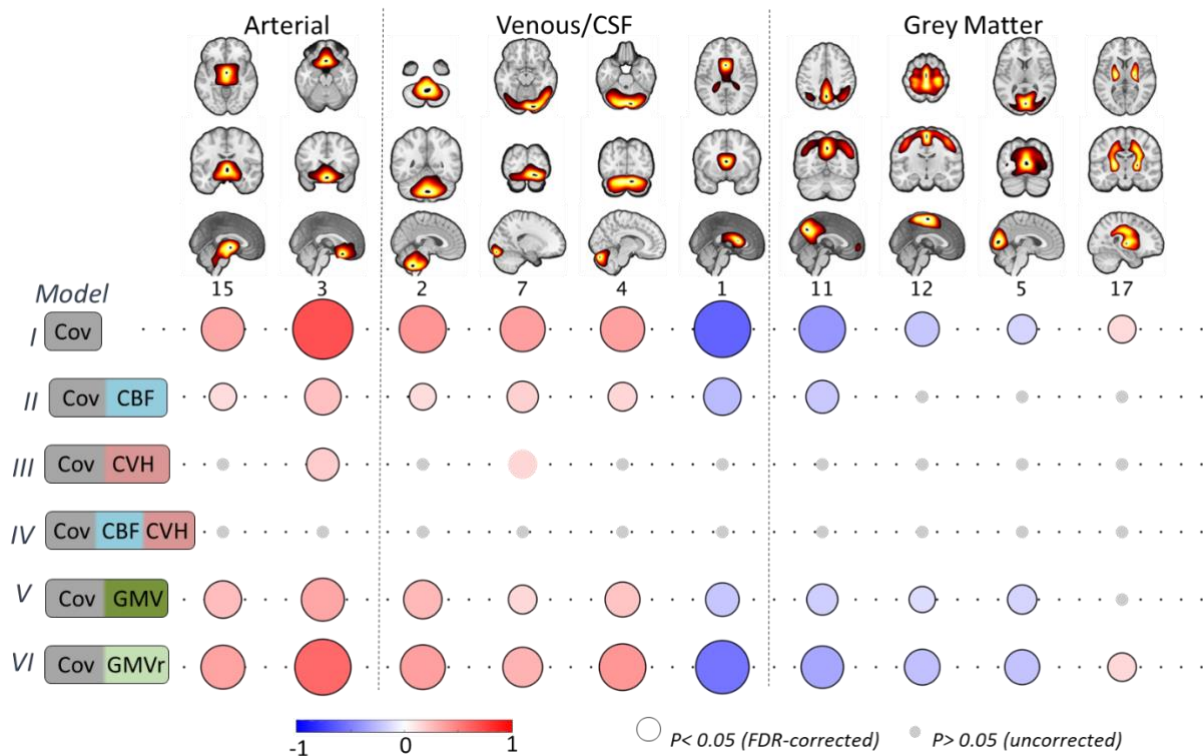
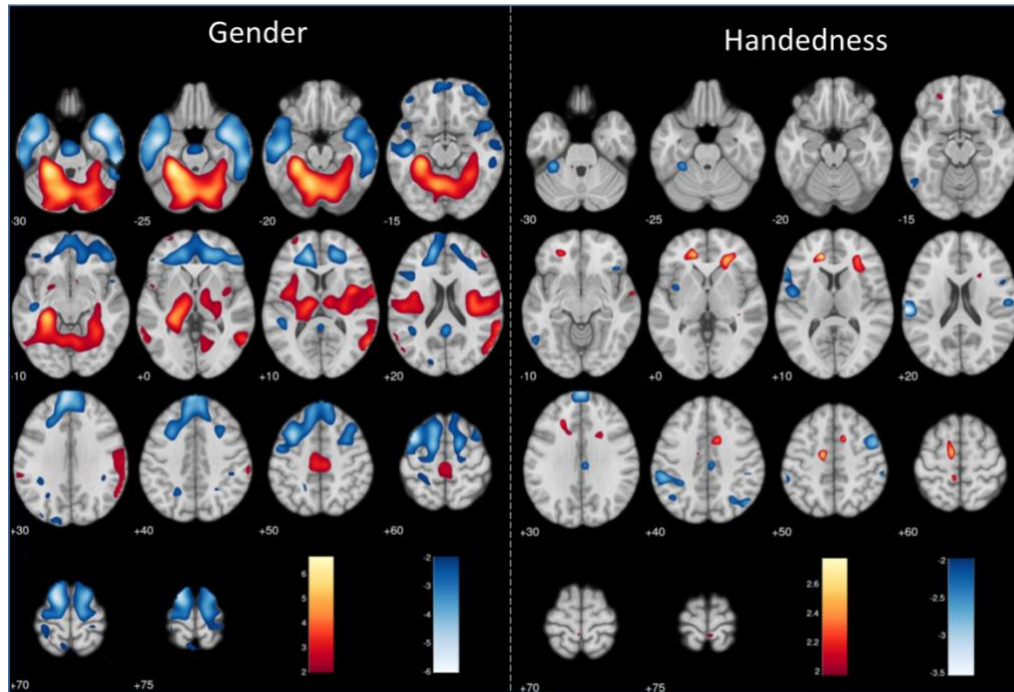
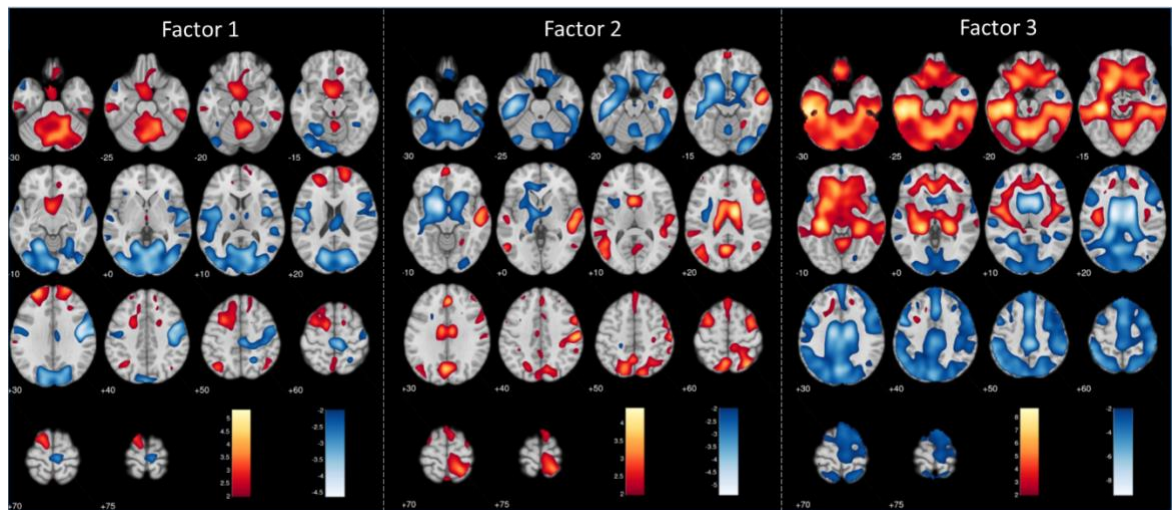


Figure 6. Component-based associations between age and RSFA residuals after controlling for: covariates only (Cov, Model I); Cov and cerebral blood flow (CBF, Model II); Cov and cardiovascular health (CVH, Model III); Cov, CBF and CVH (Model IV); Cov and grey matter volume (GMV); and Cov and grey matter volume residuals (GMVr) after controlling for the effects of CVH (see text). Grey circles denote uncorrected p -value > 0.05 , circles without black outline denote uncorrected $p < 0.05$ and circles with black outline denote FDR-adjusted p -value at 0.05.

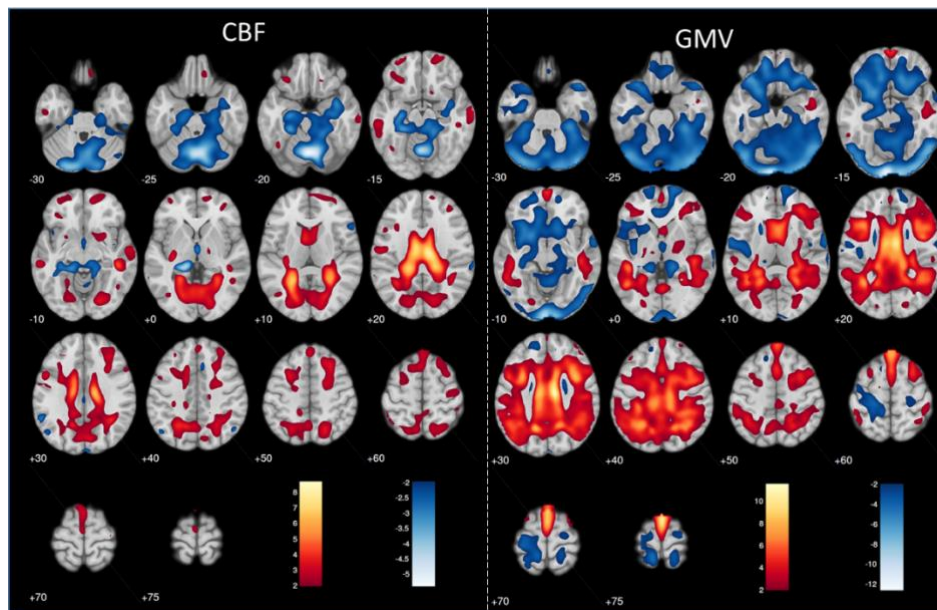
9. Supplementary Figures



Supplementary Figure 1. Voxel-wise associations between RSFA and covariates of no interests (gender – left panel and handedness – right panel), Model I. Maps are thresholded at uncorrected p -values of 0.05 for more complete description of the spatial representation.



Supplementary Figure 2. Voxel-wise associations between RSFA and three factors of cardiovascular health (Model III). Maps are thresholded at uncorrected p -values of 0.05 for more complete description of the spatial representation.



Supplementary Figure 3. Voxel-wise associations between RSFA and CBF (left panel, Model II) and GMV (right panel, Model V). Maps are thresholded at uncorrected p -values of 0.05 for more complete description of the spatial representation.